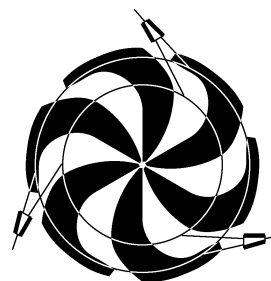# TRIUMF

ANNUAL REPORT
SCIENTIFIC ACTIVITIES
1999

**CANADA'S NATIONAL LABORATORY
FOR PARTICLE AND NUCLEAR PHYSICS**

OPERATED AS A JOINT VENTURE

MEMBERS:

THE UNIVERSITY OF ALBERTA
SIMON FRASER UNIVERSITY
THE UNIVERSITY OF VICTORIA
THE UNIVERSITY OF BRITISH COLUMBIA

ASSOCIATE MEMBERS:

CARLETON UNIVERSITY
THE UNIVERSITY OF MANITOBA
L'UNIVERSITÉ DE MONTRÉAL
QUEEN'S UNIVERSITY
THE UNIVERSITY OF REGINA
THE UNIVERSITY OF TORONTO

JULY 2000

CHEMISTRY AND SOLID-STATE PHYSICS

Experiment 677
Surface interactions and motional dynamics of free radicals in zeolites
(D.G. Fleming, UBC)

Experiment 677 is concerned with the interactions of muonated organic free radicals, especially Mu-cyclohexadienyl, MuC_6H_6, with surrounding zeolite structures. Zeolites are microcrystalline alumino-silicate structures, often incorporating extra framework cations, which have a ubiquitous presence as molecular sieves and heterogeneous catalysts in the chemical industry. Several zeolites have been studied, but the recent experiments have focused on NaY, a typical faujasite, which is an important class of zeolites having 'supercages' about 13 Å in diameter, connected by 'window' (W) sites of about 7 Å diameter.

Experiment 677 used a week of beam in M15 just before the summer hiatus, acquiring data that cleared up ambiguities in previous data, bringing out a clear picture of MuC_6H_6 in NaY zeolites. The previous data, taken over the course of Expt. 677, include FT-μSR and ALC-μSR measurements of the MuC_6H_6 radical in NaY at low to moderate benzene loadings over a wide temperature range. The recent run measured the FT-μSR spectra at several low magnetic fields, as in Fig. 64, complementing previous high-field TF measurements (Fig. 65) and ALC spectra (e.g., Fig. 66)
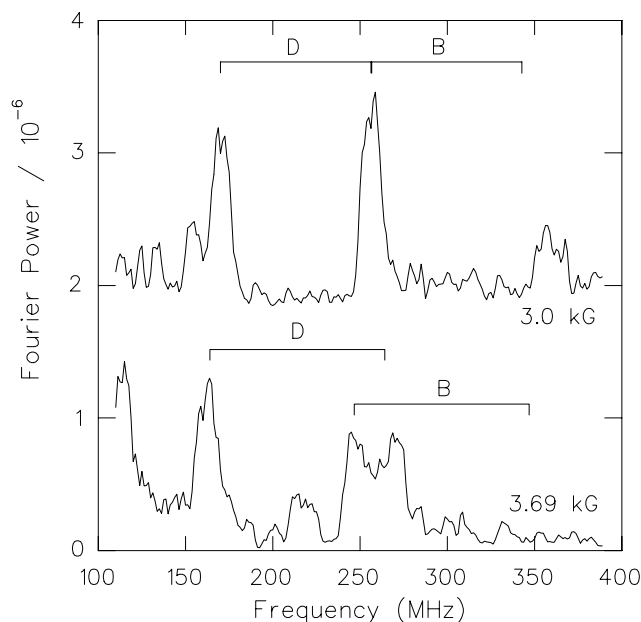

Fig. 64. Fourier power spectra for the MuC_6H_6 radical in NaY at fields of 3.0 and 3.69 kG. The much larger diamagnetic peak is at lower frequencies (41 and 50 MHz). Pairs of peaks (separated by $2\nu_{dia}$) are labelled as for the corresponding ALC peak. There are unassigned peaks that do not appear consistently over multiple runs.
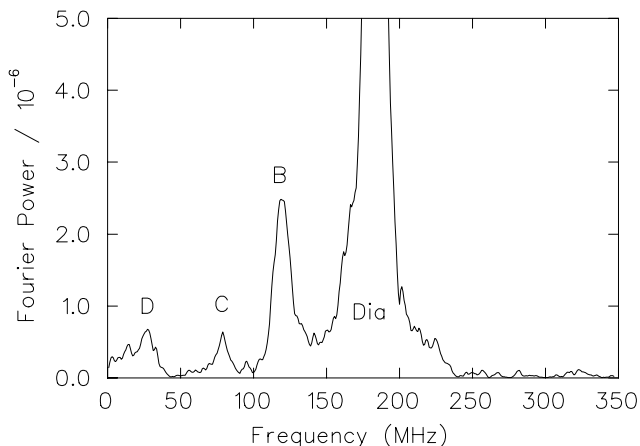

Fig. 65. Fourier power spectrum for the MuC_6H_6 radical in NaY at a field of 13.5 kG. Only one peak of each pair is visible for A, B, and C.
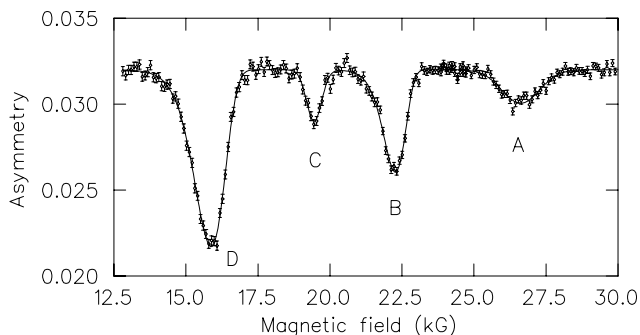

Fig. 66. Representative ALC-μSR spectrum for the MuC_6H_6 radical in NaY at 322 K. The solid line is a fit to skewed Gaussian lineshapes, in lieu of a fittable theoretical lineshape, and the background has been subtracted to show a flat baseline.

taken over the temperature range 3–322 K. The radical signals in the Fourier spectra are very weak and broad, especially at low fields (Fig. 64).

The ALC spectra show four clear broad resonances, labelled A–D in order of decreasing field. Both $\Delta M = 0$ (Δ_0) and $\Delta M = 1$ (Δ_1) transitions are expected, resulting from the isotropic and anisotropic hyperfine interactions, respectively. Since Δ_1 involves a muon spin flip, both ALC and FT should give the same muon hyperfine coupling (hfc), leading to the assignments shown in Figs. 64 and 65.

Peak A, which does not appear in Fourier spectra, is the Δ_0 transition for the $-CHMu$ group of the MuC_6H_6 radical, with peak B being the corresponding Δ_1, giving muon and proton hfcs of $A_\mu = 606 \pm 2$ MHz and $A_p = 108 \pm 2$ MHz. Both values indicate very large shifts of 15% from the bulk phase values, which we attribute to strong binding of the MuC_6H_6 radical to the Na cations (at the S_{II} site) in NaY. The temperature dependences of muon and proton hfcs are unusual, with

A_p actually increasing, albeit modestly, with increasing temperature. Both of these results point towards a non-planar equilibrium geometry for the MuC_6H_6 radical interacting with the Na cation, with the $-CHMu$ group above the plane of the ring, wherein the muon (peak B) adopts a more axial orientation away from the cation and the proton (A) an equatorial one. The fact that the muon and proton hfcs have the opposite temperature dependence can be explained if, with increasing temperature, the muon effectively moves away from the source of π electron density at the ortho carbons, while the proton moves towards this source.

Peak D gives a muon hfc of $A_\mu = 430$ MHz, which is 20% below the bulk phase, and is a clear indication of either other sites or other orientations of the $C-Mu$ bond. The obvious candidate is the W site, but that assignment implies unreasonably large hyperfine shifts for a site far removed from strong interactions with the Na cations. Thus we are inclined to the view that peak D represents the Δ_1 transition for the opposite orientation of the methylene $C-Mu$ bond at the S_{II} cation site: peak B with the muon pointing away from the cation, and peak D pointing towards. Given this result, it appears peak C would be the corresponding Δ_0 resonance, giving $A_p = 67 \pm 1$ MHz, but that is at odds with the labelling of peak C in the FT of Fig. 65 (though not visible in Fig. 64). Interpreting peak C as Δ_1 due to the W site gives $A_\mu = 525$ MHz, much the same as that in bulk benzene, as expected for the W site. Therefore, peak C in Fig. 66 may be the sum of both the Δ_0 companion for peak D and the Δ_1 peak for the W site.

In summary, the hfcs for the muon and proton of the $-CHMu$ group in two different orientations of the radical have been determined. At 322 K they are: $A_\mu(1) = 606 \pm 2$ MHz and $A_p(1) = 108 \pm 2$ MHz, for the muon on the opposite side of the ring from the cation; and $A_\mu(2) = 430 \pm 2$ MHz and $A_p(2) = 70 \pm 4$ MHz, for the muon on the same side. The MuC_6H_6 radical in the window site was likely also observed to have $A_\mu = 525$ MHz.

Experiment 684
μSR spin relaxation studies of small molecules in the gas phase
(J. Pan, D. Fleming, UBC-TRIUMF)

This experiment studies the muon spin relaxation in some simple gas-phase systems with the primary goal of measuring the chemical reaction rates. Due to varying factors, including the loss of beam time as a result of the cyclotron shutdown, only one week of the experiment was carried out for the study of Mu + CO with He as moderator at room temperature.

The motive is to complete the survey of the Mu + CO reaction with He moderator over a wide range of pressures from 2 to 500 bar. Particularly, the recombination reaction rate constants of Mu + CO have shown marked quadratic curvature at room temperatures (and low temperatures) for both N_2 and Ar over this pressure range, but the data for He at higher pressures (>120 bar) is not conclusive although it appears to be linear.

The experiment was conducted on M15 with LAMPF in both LF and TF orientation. The target cell had a capacity to sustain up to 60 bar gas pressure.

In TF, data were taken at 5 G and 56 G magnetic field with He pressures being 10, 20, 40 and 60 bar and CO pressures being 20, 50, 100, 200, 300 torr in the cell. The results are shown in Fig. 67 along with previous high pressure data. The crosses are low field data and the diamond crosses are high field data.

The total rate constant is fairly flat at lower pressures but nonetheless increases with pressure. Fit together with high pressure data, the linear and quadratic components are compatible in magnitude. The result is then consistent with those for N_2 and Ar. The flat contribution, presumably from the rotational relaxation of the intermediate MuCO radical, is 0.41×10^{-12} cm^{3}s^{-1}.

Another interesting result is that the rate increase from lower field to higher field is not as large as expected. The ratio of rates at 6 and 56 G drops slightly over the pressure range, from 1.3 to 1.2. But the absolute separation, i.e. $k_{\text{eff}}(56 \text{ G}) - k_{\text{eff}}(5 \text{ G}) = 0.16 \times 10^{-12}$ cm^{3}s^{-1}, remains fairly constant throughout.

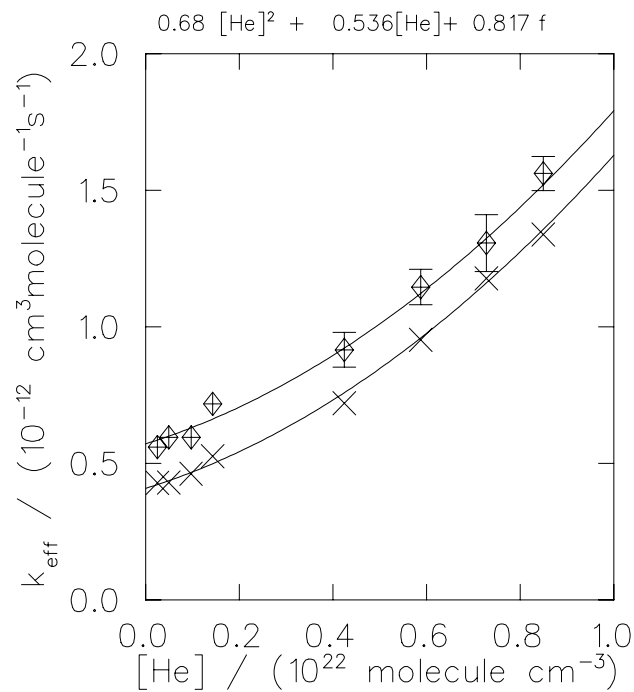Fig. 67. Mu + CO + He at room temperature.

If the separation is entirely from the electron spin-flip contribution, then $k_{sf} = 0.16 * 2 = 0.32 \times 10^{-12}$ cm^{3}s^{-1}.

In LF, measurements were made with selected gas mixtures at 1.0, 1.7, 2.8 and 3.7 kG.

One outstanding question about the mechanism of this reaction is whether the field decoupling constant equals that of the Mu or MuCO radical. The LF data obtained can be fit very well to the normal $1/(1 + x^2)$ decoupling formula with the Mu hyperfine coupling constant. In addition, the slopes of the above fits depend linearly on [CO] independent of the He pressure, while the intercepts of the above fits depend linearly on both [CO] and [He]. This is consistent with a spin-flip type reaction mechanism on top of a termolecular chemical reaction. The spin-flip reaction rate constant calculated from the slope is 0.42×10^{-12} cm^{3}s^{-1}, consistent with the values obtained in TF (0.41 or 0.32).

The overall conclusions are, first there is a constant contribution from electron spin-flip relaxation over the pressure range; secondly, there is a large spin relaxation contribution at lower pressures that does not behave like spin exchange; finally, the chemical rate constant is likely not linearly dependent on [He] but there is a large linear component, unlike in the case of Mu + CO+ N$_2$. The "flat" intercept seems to suggest that the correlation time τ_c is constant over the lower pressure range. A first-order model calculation yields a termolecular rate constant at 1.5×10^{-34} cm^6 s^{-1}. This can be compared with the corresponding value for Mu + NO + He, 7.7, reflecting the larger chemical barrier for HCO.

Experiments 713 and 842
Muonium chemistry in supercritical water
(P.W. Percival, SFU)

Experiment 713 was conceived to explore the potential of μSR to probe chemistry in supercritical water, using muonium as a model for the hydrogen atom. The original aim was so well satisfied that a second proposal, Expt. 842, was launched to pursue some of the new lines of research uncovered by Expt. 713. This report covers the 1999 activities of the combined project.

The motivation to study chemistry in supercritical and near critical water stems from the remarkable changes that occur as pressure and temperature are raised to, and past, the critical point (374°C, 221 bar). Supercritical water (SCW) behaves more like an organic solvent than the high dielectric, hydrogen-bonded liquid that exists under standard conditions. Not surprisingly, this has profound effects on the chemistry of aqueous solutes, and this has resulted in several novel applications. Perhaps the most significant of these is the development of supercritical water oxidation (SCWO) reactors as a means for the destruction of hazardous organic materials, such as chemical weapons. There are significant engineering problems in processing large volumes of material at very high temperatures and pressures, but these have been largely overcome. What is missing is detailed information at the microscopic level – reaction mechanisms, intermediates, and chemical rate constants.

Since muonium behaves chemically as a light isotope of hydrogen, it can be used to study H atom chemistry and the properties of free radicals which incorporate H (almost all organic free radicals). Conventional spectroscopic tools for studying atoms and free radicals are very difficult or impossible to employ with the high temperature, high pressure apparatus needed for SCW. On the other hand high momentum muons (beam line M9B) can penetrate the window of a pressure vessel, and a large fraction of the decay positrons (whose asymmetry carries the spectroscopic information) can pass through the cell walls.

We have demonstrated the ability to study muonium in water over continuous ranges of pressure and temperature from standard conditions to over 400 bar and 400°C, corresponding to water densities from 1.0 g cm^{-3} down to 0.1 g cm^{-3}. This work was published this year [Phys. Chem. Chem. Phys. **1**, 4999 (1999)]; a second publication [Physica B, in press (2000)] reports the determination of muonium hyperfine constants over the same range of conditions. These papers are a very significant contribution to the literature, since there is no equivalent data for H or other hydrogen isotopes.

During 1999 we concentrated on measurements of muonium decay rates in dilute aqueous solutions, to determine muonium rate constants. These studies were motivated by the strange results of the preliminary investigation reported for Expt. 713 in the 1998 TRI-UMF Annual Report. It was found that the rate constant for the Mu + Ni^{++} spin exchange interaction increases with temperature at a rate less than that predicted for a diffusion-limited process, and then falls with further increase in temperature. This remarkable effect could have important consequences if found to be general, since the rates of chemical reactions are obviously important to the efficiency of SCWO destruction facilities. Even more direct is the implication for H atom reactions in the cooling water cycles of pressurized water nuclear reactors. The H atom is a primary product of the radiolysis of water, and is also produced by the combination of hydrated electrons with aqueous protons. Existing models for high temperature water radiolysis rely on extrapolation of lower temperature data [Elliot, Rate Constants and G-values for the Simulation of the Radiolysis of Light Water over the Range 0–300°C, AECL Report, AECL-11073 (1994)]. There is indication of curvature in the temperature dependence of some H atom rate constants, but the existence of

a maximum with temperature has never before been observed.

To test the generality of the effect we picked different types of reactions for detailed study. The rate constant for muonium reaction with hydroquinone is almost as high as that for Ni^{++} at room temperature, and both are at or close to the diffusion limit, i.e. the situation where reaction is very fast once the reactants come together in solution, so that the diffusion process itself is the rate-limiting step. Muonium interacts with Ni^{++} through spin exchange of unpaired electrons, so the rate can be taken as a measure of the encounter rate. In contrast, the interaction with hydroquinone is a true chemical reaction (addition of Mu to the aromatic ring of 1,4-dihydroxybenzene). Nevertheless, the results are similar (Fig. 68) – the rate constant goes through a broad maximum at subcritical temperatures.

The reaction of muonium with the hydroxide ion, OH^-, is relatively slow at room temperature and very similar to the equivalent reaction between H and OH^-. It was chosen as an example of an activated reaction by Walker *et al.* [TRIUMF Expt. 157] in a study of muonium kinetics at standard pressure. As can be seen from Fig. 69, we have extended measurements through several orders of magnitude. The diffusion-limited region ($k \geq 1 \times 10^{10}$ $M^{-1}s^{-1}$) is reached at temperatures around 300°C. At still higher temperatures there is an abrupt drop in rate constant. The data in this region are very sensitive to pressure, and this contributes to the apparent scatter of points above 350°C. It seems as if the "drop off" temperature is displaced to higher values at higher pressures, consistent with the interpretation that the solvent density is a key factor in the efficiency of diffusion-limited reactions. The "drop off" marks the threshold between conventional liquid behaviour, where reactants undergo multiple encounters in the solvent cage, and gas-like behaviour, where the mean free path between collisions is relatively high.
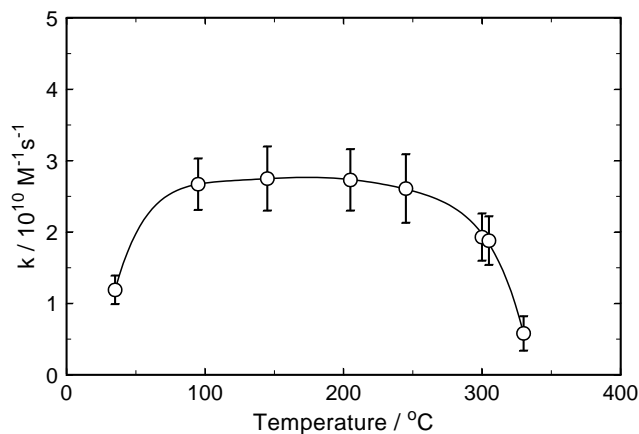

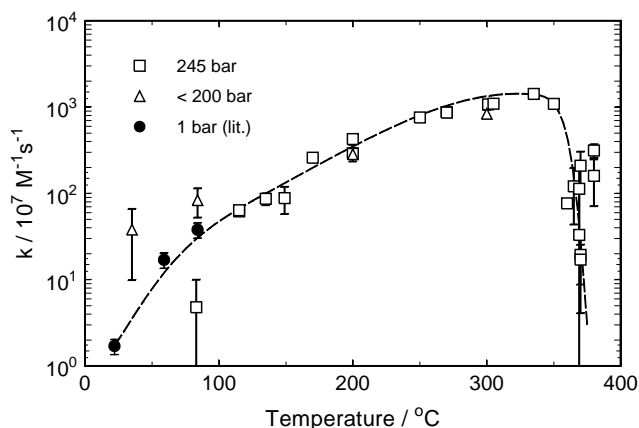Fig. 68. Rate constants for Mu + hydroquinone in water at 245 bar.

Fig. 69. Rate constants for Mu + hydroxide in water. Note the logarithmic scale. The literature data is taken from Ng *et al.* [J. Phys. Chem. **88**, 857 (1984)].

The third reaction reported here, Mu + I^-, is unusual in its apparent negative activation energy, which was also found for H and D atoms [Bartels and Roduner, Chem. Phys. **203**, 339 (1996)]. Since one explanation proposed for this strange kinetic behaviour involved solvent effects on the transition state, we decided to test this by extending measurements to the high temperature region, where we have already noted the transition to gas-like behaviour. Our current data (Fig. 70) does indeed show a reduction in the slope of the temperature dependence, consistent with the expected reduction in a dynamic solvent effect. We plan to go to higher temperatures in future beam time.
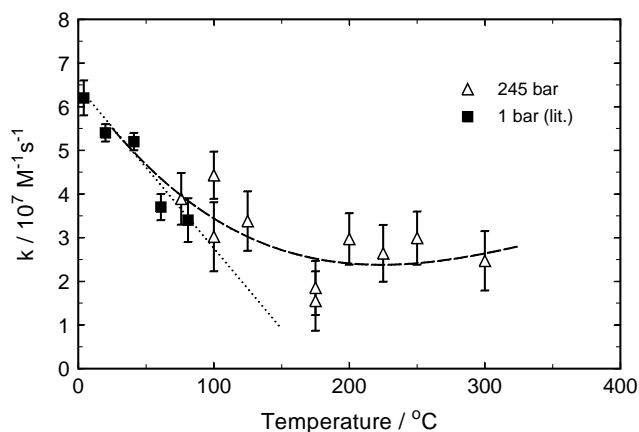

Fig. 70. Rate constants for Mu + iodide in water. The literature data is taken from Bartels and Roduner [*op. cit.*].

Experiment 746
Muonium in Si
(S.R. Kreitzman, B. Hitti, TRIUMF)

The work reported here is a continuation of previous studies directed at furthering the understanding of muon, and hence hydrogen, dynamics in Si. Previous stages of the work have investigated transitions among

66

the muon charge states, interactions with band electrons and holes arising from dopant impurities, and muon site transitions. Much of that research has relied on RFμSR methods which are equally sensitive to both the so-called prompt and the final states of the muon. That is to say, RFμSR can measure the muon states that form immediately after implantation and also those states which take some (reaction) time to appear. Indeed the strength of the RFμSR method is the fact that final states are accessible. The carbon lining is, however, a possible ambiguity, particularly if no obvious criteria exist which tell one which state is prompt and which is final.

To help solve this problem, one can turn to traditional transverse field (TF) μSR, a technique with very well known criteria that allows the identification of whether a signal is coming from a prompt or final state. The utility of this TF feature for the current investigation is apparent in Fig. 71 (reproduced from previous data) where the RFμSR hyperfine frequencies for tetrahedral muonium in Si are displayed. We see that two distinct Mu frequencies appear below 20 K. The data, however, do not distinguish which (if any) frequency represents a prompt or a final state.

To resolve this situation a set of TF runs were taken in the Belle high timing resolution apparatus (necessitated by the very high frequencies produced by tetrahedral muonium in Si). An example at 10 K is shown in Fig. 72; here the TF data also show a split line. Detailed analysis surprisingly shows that the lower frequency line in Fig. 72 (which corresponds to the lower branch in Fig. 71) is the prompt fraction, whereas the upper branch arises from delayed formation. Perhaps it is not too surprising that given both prompt and delayed fractions at low temperature, the high temperature data seem continuous (and therefore identified) with the delayed fraction.
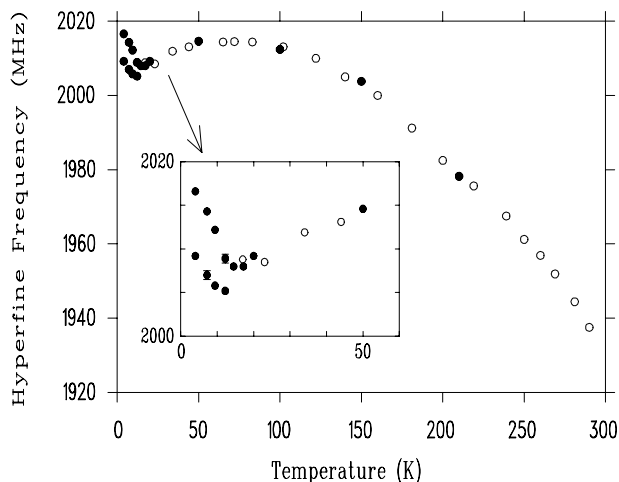

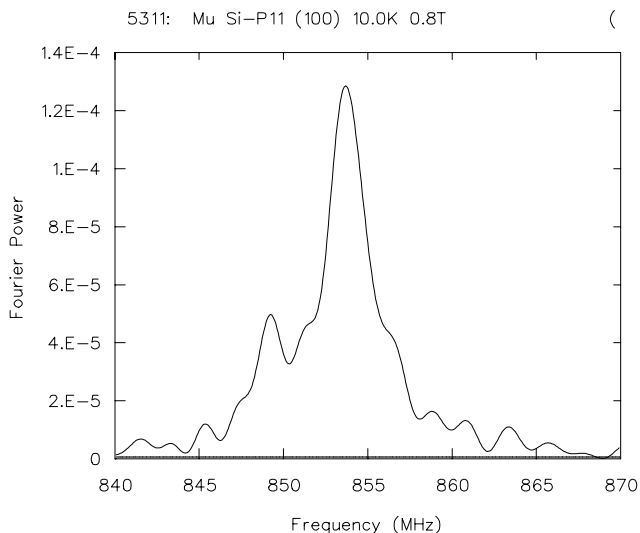Fig. 71. The Mu_T^0 hyperfine frequency in Si as a function of temperature using the RFμSR method.

Fig. 72. The Mu_T^0 transverse field signal at 10 K in 0.8 T.

Experiment 749
Muonium-substituted free radicals
(P.W. Percival, SFU)

Addition of muonium to an unsaturated molecule results in a free radical incorporating the muon in place of a proton. Thus, muon irradiation of benzene results in the cyclohexadienyl radical, C_6H_6Mu. Muon hyperfine constants are determined by the transverse-field muon spin rotation technique (TF-μSR) and other hyperfine constants by muon level-crossing resonance (μLCR). The hyperfine constants usually allow unambiguous identification of the free radicals.

One of the goals of Expt. 749 has been to understand the factors that influence radical addition to curved polyaromatic hydrocarbons (PAHs). The significance of this issue can be seen by considering the addition of H atoms or other small radicals to fullerenes. There is a single radical product in the case of C_{60}, since all carbons are identical. In contrast, the ellipsoidal C_{70} molecule has five chemically inequivalent sets of carbon atoms. In principle, therefore, five distinct radicals could be formed. Their abundances are in direct proportion to the reactivity of the different carbon sites.

We have investigated this matter by using TF-μSR to detect muonium adducts, i.e. $C_{70}Mu$, and were able to distinguish four isomeric radicals. Our findings agree with ESR studies of H adducts, but Prassides *et al.*, working at PSI, claim that a weak feature in the μSR spectrum is the elusive fifth radical. If it exists at all, it is only in very low abundance. The radical in question corresponds to addition to the "equator" of C_{70}, the least curved part of the ellipsoid. To test the reactivity of "flat" PAHs we investigated the Mu adducts of pyrene [Percival *et al.*, Can. J. Chem. **77**, 326 (1999)].

Three radicals were identified, but all are formed by Mu addition to the edges of the planar carbon network that comprises pyrene. No evidence was found for addition at the carbon sites which most resemble those of a fullerene.

During 1999 we continued the next step in the project, the study of Mu addition to 1,8-dioxa[8](2,7)pyrenophane. As can be seen from Fig. 73, the pyrenophane differs from pyrene by the presence of an alkyl chain which joins together opposite ends of pyrene and thus imposes curvature on the molecule. This novel molecule was synthesized in the laboratory of Gra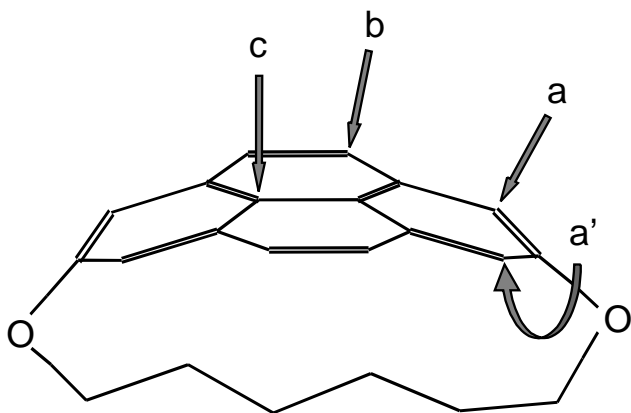ham Bodwell of the Memorial University of Newfoundland. There are three classes of carbon sites available for radical addition; examples are labelled **a**, **b**, and **c** in Fig. 73. However, each of these sites might be attacked from the top or bottom, as indicated by the arrows for **a** and **a'**. The direction of attack does not matter for pyrene, which is planar, but for pyrenophane there are distinct *exo* and *endo* adducts.

We have predicted hyperfine constants for all six possible radicals by means of density functional calculations on model systems (radical structures without the alkyl chain, but with fixed curvature of the carbon frame). As previously reported in the 1997 TRIUMF Annual Report, only two radicals are evident in the TF-μSR spectrum. Their muon hyperfine constants, 295.4 MHz and 391.0 MHz, narrow the choice of possible radical isomers formed in this system, but a detailed match of the predicted proton couplings with values derived from the μLCR spectrum is necessary for reliable identification.

The data collected in 1997 revealed several strong LCR signals, but also others with amplitudes close to the noise level. Therefore part of the spectrum was scanned again in November, 1999. Figure 74 displays the most significant portions of the new data – note the broken axis. Further analysis is necessary to combine the data from the two run periods and confirm or eliminate some weak features. However, considering only the strongest resonances, it seems most likely that muonium adds to pyrenophane to give the two *exo* radicals indicated by arrows **a** and **b** in Fig. 73.

Fig. 73. 1,8-dioxa-[8](2,7)pyrenophane. The arrows point to three types of carbon atoms where radical addition is likely. Each site may be attacked from above or below, as indicated by the **a'** example.
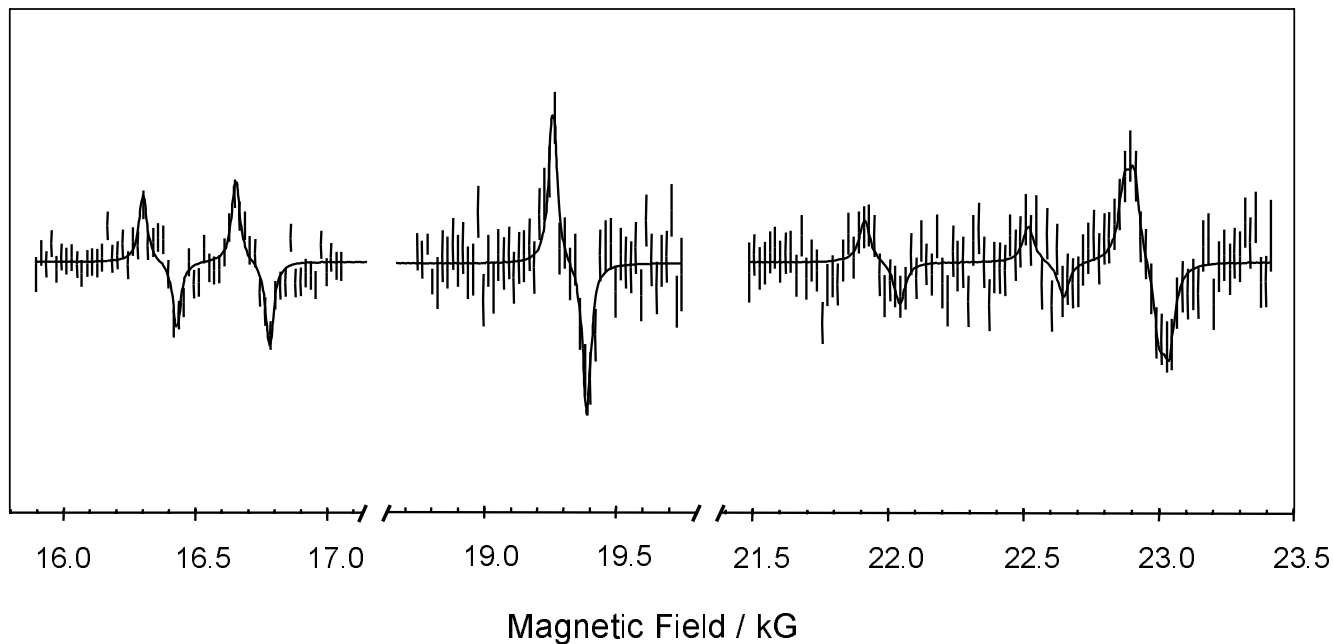

Fig. 74. Part of the avoided level-crossing spectrum obtained for a solution of pyrenophane in tetrahydrofuran.

Experiment 774
Muonium dynamics in GaAs
(B. Hitti, S.R. Kreitzman, TRIUMF)

Hydrogen in semiconductors is an important impurity which can alter the electrical and optical properties of these materials. Experiments on isolated hydrogen are not practical and since the muon is an electronic analogue of the proton, the various techniques of muon spin rotation/relaxation (μSR) can be used to extract the relevant information. What distinguishes Expt. 774 from earlier μSR work on GaAs is that it is the first such experiment to be performed on high quality liquid phase epitaxy (LPE) samples. Standard fabrication of GaAs introduces a large defect population. At the low dopant concentration where the basic dynamical processes are best revealed, our results show that the use of structurally defect free material (LPE samples) is essential to study intrinsic processes.

To date we have used the radio frequency (RF)μSR technique to measure the temperature dependence of the diamagnetic fraction at 2 kG in a number of samples between 10 K and 650 K, Fig. 75. At low temperature the data measured on the LPE semi-insulating (SI) substrate (Fig. 75a) has the simplest temperature dependence. From earlier work we can tentatively attribute the sharp rise in the amplitude just below 100 K to the ionization of Mu_{BC}^0 and the increase observed above room temperature to the ionization of Mu_T^0. The two commercial samples, Sumitomo and MCP, are high resistivity well compensated samples. Figure 75b shows a peak at 50 K and ambiguous structure at 100 K, which are attributed to the presence of structural
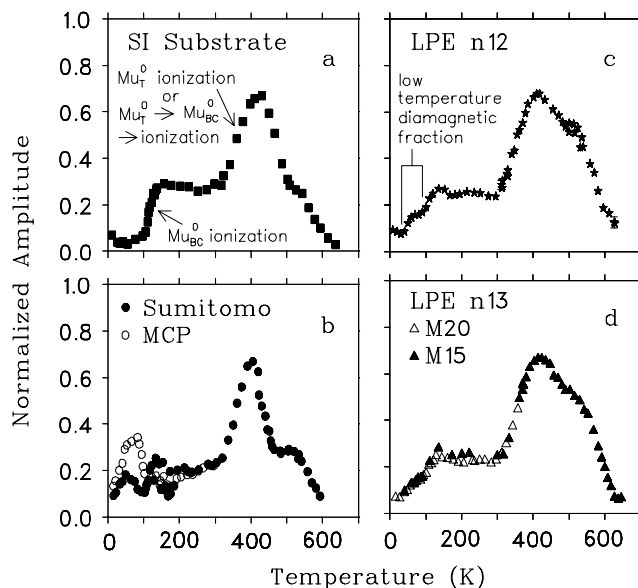

Fig. 75. The temperature dependence of the diamagnetic amplitude in the various semi-insulating and n-type LPE samples studied so far with the RF μSR technique.

defects and impurities. The two LPE samples n12 (carrier concentration 2×10^{12} cm^{-3}) and n13 (2×10^{13} cm^{-3}), Fig. 75c and Fig. 75d, show a much slower increase in the amplitude and a larger diamagnetic fraction at low temperature when compared to the SI substrate. While this is clearly related to the availability of electrons in the doped material, the exact mechanism is not yet understood.

The diamagnetic amplitude in all samples reaches its largest value at about 400 K. At higher temperatures all samples show a drop in the amplitude which is attributed to the charge exchange cycle involving the diamagnetic state and free electrons. As seen in Figs. 75a and 75b the SI samples show two drops, one centred around 450 K and the second around 575 K. The drop centred at 450 K may result from the ionization of the mid-gap double donor EL2 centres, present in commercial samples. The LPE samples are free of this defect so the much weaker decline in those materials is not yet understood; one possibility will be investigated during the next beam period. The higher drop centred at 575 K is consistent with the size of the GaAs band gap and the expected charge exchange involving conduction electrons.

Experiment 776
Rare-earth materials with disordered spin structures
(D.R. Noakes, Virginia State)

This experiment is a muon spin relaxation (μSR) study of RE-Mg-Zn (RE = rare earth) quasicrystals and PrP$_x$ induced moment "spin glasses", motivated by the common features in the results of Expt. 665 (Al-Mn-Si quasicrystals) and Expt. 640 (low-carrier-density Kondo-lattice CeNiSn and related materials). Study of the rare earth quasicrystals was basically completed, with the discussion in the previous Annual Report. Our final paper addressing μSR in quasicrystals has now appeared in J. Phys. Cond. Matter [Noakes, **11**, 1589 (1999)]. Since the results of that paper are also relevant to Expt. 797, it is also discussed in the report on that experiment.

A paper describing the surprising observation of strong-collision-dynamic Lorentzian Kubo-Toyabe relaxation in PrP$_x$, as discussed in the previous Annual Report, was presented at the International Conference on μSR held in Switzerland in September. This will be published in the proceedings of the conference in Physica B.

That paper includes our singlet ground state crystalline electric field (CEF) fluctuation model for the system, but detailed explanation of the temperature dependence of the dynamic Lorentzian Kubo-Toyabe fit parameters was not achieved. To better understand

the temperature dependence of the local fields at the muon site generated by the model, we are constructing a microscopic Monte Carlo simulation of the ion CEF fluctuations on a cluster of Pr ions in the PrP structure. This will use much of the code of our previous publications on Monte Carlo simulation of static local fields at muon sites [Phys. Rev. **B44**, 5064 (1991); Noakes, *op. cit.*], but now moment dynamics will be included in the calculation as well.

Experiment 783
Paramagnetic frequency shifts in unconventional superconductors
(R.H. Heffner, J.E. Sonier, LANL)

In 1999 we carried out muon Knight shift measurements in recently available single crystals of the heavy-fermion superconductor $U_{0.965}Th_{0.035}Be_{13}$. This system and the parent compound UBe_{13} are of widespread interest because of their unidentified superconducting phases. In the thoriated compound there are two known phase transitions which occur upon decreasing the temperature. Although the first transition T_{c1} is known to be a superconducting transition, little else is known – including the symmetry of the superconducting pair wavefunction. There is even less known about the lower temperature transition T_{c2}. In particular, it has not been established whether this transition is associated with a new superconducting phase or the onset of strong magnetic correlations. A small internal magnetic field was detected in earlier zero-field μSR measurements on polycrystalline samples of $U_{1-x}Th_xBe_{13}$ for the thorium concentration range $0.019 < x < 0.045$ [Heffner *et al.*, Phys. Rev. Lett. **65**, 2816 (1990)]. However, there are several possible origins of this magnetism. These include the formation of a spin-density wave instability, the formation of true long range antiferromagnetic correlations, or the formation of a superconducting state that breaks time-reversal symmetry.

Figure 76 shows the temperature dependence of the muon Knight shift in $U_{0.965}Th_{0.035}Be_{13}$. The measurements were carried out on the M15 surface muon channel in an applied magnetic field of $H = 10$ kOe. Due to the dipolar fields associated with the localized U $5f$-moments, there are two magnetically inequivalent muon sites. In the superconducting state (i.e. below $T_{c1} \approx 0.5$ K) the change in the Knight shift reflects the change in the electron spin susceptibility χ_s due to the formation of Cooper pairs. For the case of a conventional superconductor with orbital s-wave ($L = 0$) spin singlet ($S = 0$) pairing, χ_s vanishes as the temperature is reduced to $T = 0$ K. A preliminary analysis shows that χ_s decreases below T_{c1} and becomes temperature independent below T_{c2}. The latter behaviour is not yet understood. An additional observation is that
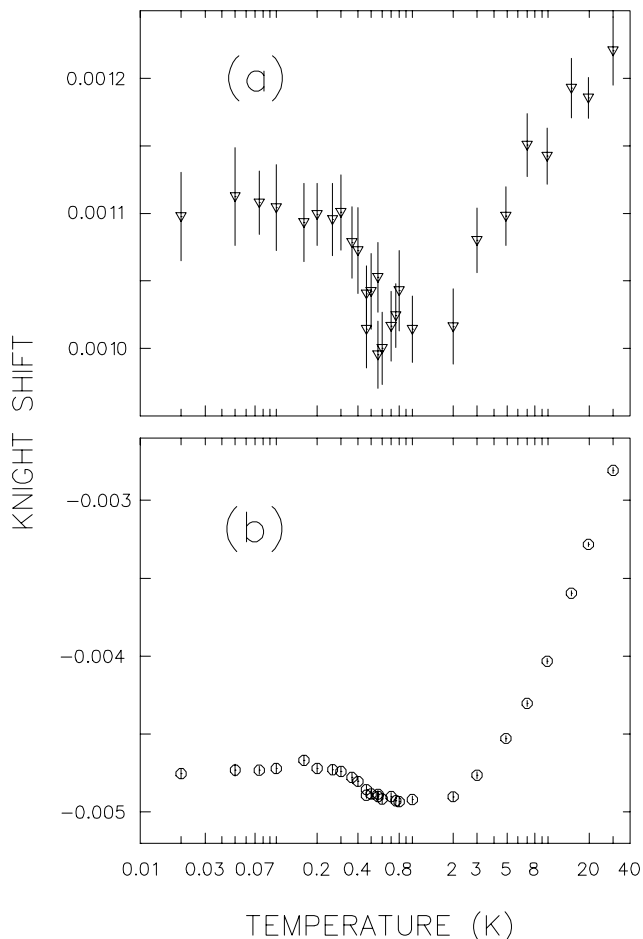

Fig. 76. The Knight shift for the two magnetically inequivalent muon sites in single crystal $U_{0.965}Th_{0.35}Be_{13}$ measured in an applied field $H = 10$ kOe.

the transferred hyperfine coupling between the muon spin and the U $5f$-electrons is temperature dependent and anisotropic. This is presumably due to the detailed nature of the hybridization between the U $5f$-electrons and conduction s-electrons.

Experiment 791
Electronic structure and dynamics of charged muonium centres in semiconductors
(K.H. Chow, Lehigh; R.F. Kiefl, UBC; B. Hitti, TRIUMF)

Results of experiments on muonium in semiconductors are generally considered to be the main source of information on *isolated* hydrogen in semiconductors. Hydrogen is an important impurity which can dramatically affect the electrical and optical properties of these technologically relevant materials. As reported in last year's Annual Report on Expt. 791, we recently turned our attention to studying muonium in heavily doped p-type GaAs with the intention of addressing the issue of passivation, i.e. formation of muonium-impurity complexes. Observing and understanding this process "as-

it-happens" at the microscopic level using μSR would provide new insight into how passivation occurs which is unobtainable using other techniques used to investigate hydrogen.

Our recent results are very exciting. We investigated three highly doped samples of p-type GaAs:Zn with Zn concentrations of 4.5×10^{18} cm^{-3}, 1.0×10^{19} cm^{-3}, and 2.5×10^{19} cm^{-3}. These measurements are summarized in Fig. 77, which shows the temperature dependence of the decay (assumed to have a Gaussian functional form) of the muon polarization taken under zero-field conditions.

The results can be interpreted as follows: The initial flat region up to $\approx$200 K confirms that the implanted Mu$^+$ is immobile in this temperature region. The subsequent decrease in the relaxation is due to the muon becoming mobile. By about 550 K, the muon reaches a trap and is essentially static there. Note the region between 300 K and 550 K. At any temperature, the more heavily doped the sample, the larger the relaxation. The most reasonable explanation is that the muon reaches a trap site "sooner" as the dopant concentration is increased, as would be expected if the muon were forming a complex with a Zn dopant atom. Above 550 K, breakup of the complex occurs and the muon diffuses freely through the lattice. Another regime appears above 800 K. At these temperatures, charge state changing reactions occur because a sufficient number of free electrons are being thermally generated. In this case, the reaction of relevance is cyclic, Mu$^+$ $\leftrightarrow$ Mu^0, probably involving alternating electron/hole capture. The transition from Mu$^+$ to Mu^0 occurs via capture of an electron and should be the slower of the two reactions. In such a situation, the muon depolariza-

tion is governed by the rate of this step. Consistent with this model, at any temperature, the more heavily doped the sample (the smaller the free electron concentration), the smaller the relaxation rate.

Through the use of the level crossing technique, we have also investigated the electronic structure of the muon-dopant complex formed near 500 K. The details of this study, as well as a more detailed discussion of the dynamics outlined above, will appear in an upcoming publication currently in preparation.

Experiment 797
Magnetic correlations in the ternary compounds CeTSn
(A. Kratzer, Tech. Univ. Munich)

CeNi$_{1-x}$T$_x$Sn with T = Cu, Pt

The special physical properties of CeNiSn are explained in terms of a rather narrow pseudo-gap ($\sim$5 MeV) in the density of states near the Fermi level and a spin gap in the spectrum of coherent antiferromagnetic excitations which develop at low temperatures. Previous μSR work has shown that magnetic order (including spin freezing) is absent down to $\sim$15 mK due to the dominance of coherent spin fluctuations caused by the Kondo interaction with $T_{\mathrm{Kondo}} \approx 25$ K. The pseudo-gap originates from the hybridization of the Ce $4f$ electrons with the conduction band. The hybridization strength is coupled to the unit cell volume. The increase of volume by 5–6% leads in CePtSn and CePdSn to metallic behaviour and (complex) antiferromagnetic order at $T_N \approx 7.5$ K. A continuous expansion of unit cell volume can be induced by forming pseudo-ternary compounds such as CeNi$_{1-x}$Cu$_x$Sn or CeNi$_{1-x}$Pt$_x$Sn. These compounds will attain some type of magnetic order (or spin freezing) when exceeding a certain critical concentration x_c.

We have recently studied the regime around the critical concentration by a combination of μSR and specific heat measurements, especially in the case of CeNi$_{1-x}$Cu$_x$Sn. The onset of magnetism is detected with μSR by a sharp rise in relaxation rate. The temperature at which this rise in rate occurs is taken as the magnetic transition temperature whose dependence on lattice expansion is depicted in Fig. 78. The critical value is much, much lower if Ni is replaced by Cu (ΔV $\sim$ 0.7% at $x_c \sim$ 7%) than in the case of replacement by Pt (ΔV $\sim$ 1.5% at $x_c \sim$ 30%). Evidently, unit cell volume is not the only parameter controlling the appearance of magnetism in these materials. The difference in replacing Ni with Cu or Ni with Pt is that in the former case additional $3d$ electrons are introduced into the system. It appears that $3d$ electron density is another parameter influencing magnetism in those intermetallics.
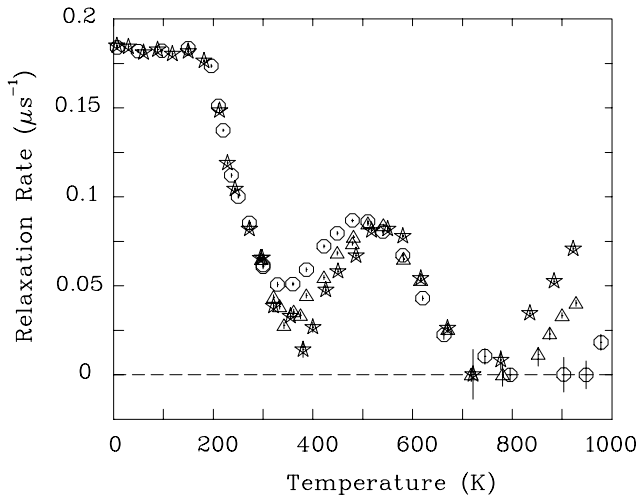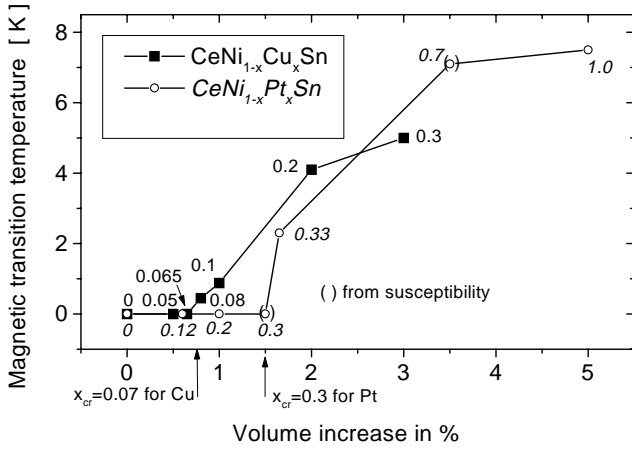

Fig. 77. Gaussian relaxation rate as a function of temperature in p-type GaAs:Zn samples. The circles represent the 2.5×10^{19} cm^{-3} sample, the triangles the 1×10^{19} cm^{-3} sample, and the stars the 4.5×10^{18} cm^{-3} sample studied under zero-field conditions.

Fig. 78. Variation of magnetic transition temperatures (temperature where a sharp rise in relaxation rate occurs) with volume increase for $CeNi_{1-x}Cu_xSn$ and $CeNi_{1-x}Pt_xSn$. The numbers at the data points give the values of x (italics refer to the Pt case).

None of the compounds with $x \geq x_c$ exhibited a spontaneous spin precession signal. The magnetic μSR response was always a nearly-monotonic loss of muon spin polarization, which seems to be characteristic of some highly disordered magnets. To fit this type of spectra, a special function termed Gaussian broadened Gaussian relaxation was developed. It has been shown recently (see last paragraph of this report) that this type of relaxation behaviour is intimately coupled to spatial magnetic inhomogeneities in the material such as regions with different sizes of the (Kondo-compensated) magnetic moment. This analysis allows extraction of a correlation length for those regions of inhomogeneity, which in the present case was on the order of 12 Å (or three mean Ce–Ce separations).

The question arises whether this disappearance of magnetic order at x_c can be regarded as a quantum critical point. If this notion is correct, the system should exhibit so-called 'non Fermi liquid' (NFL) behaviour just below x_c. One characteristic feature of NFL behaviour is a logarithmic divergence of C/T for $T \to 0$, with C being the specific heat. Data for a single crystalline material with $x = 0.05$ show indeed a strong upturn of C/T on moving towards $T = 0$. This upturn follows roughly, but not precisely, a logarithmic dependence. A better description is an algebraic temperature dependence $C/T \propto T^{-\alpha}$ with $\alpha = 0.29$. This type of behaviour was predicted for magnetically strongly disordered systems near a magnetic instability within the frame of a 'Griffith phase' scenario, originally developed for spin glasses. This result provides good evidence that quantum critical behaviour governs the onset of magnetism in the vicinity of x_c for $CeNi_{1-x}Cu_xSn$. The critical region for $CeNi_{1-x}Pt_xSn$ is at present not well enough defined for a study of

AFM = antiferromagnetism   PM = paramagnetism
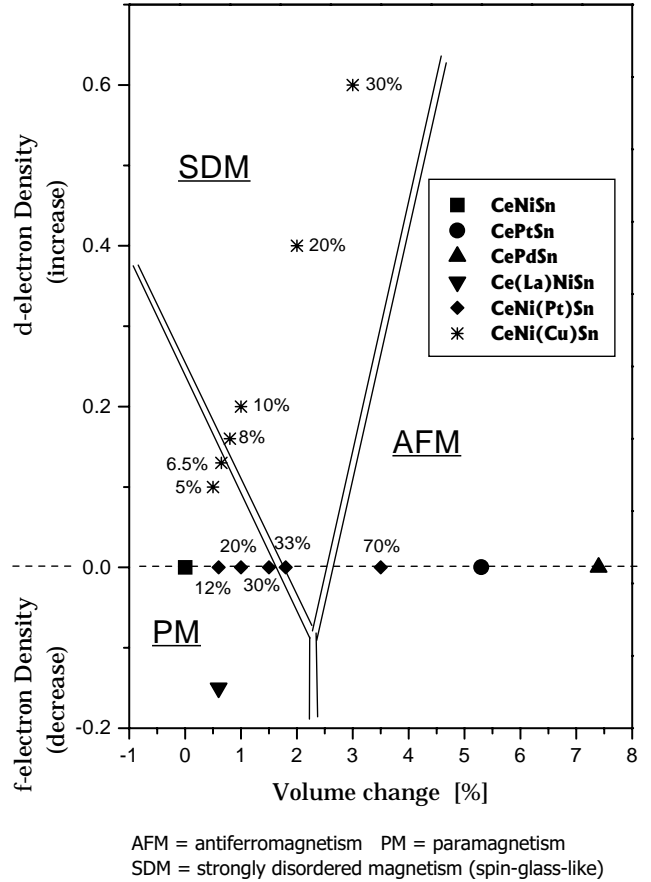SDM = strongly disordered magnetism (spin-glass-like)

Fig. 79. Provisional magnetic phase diagram for the CeTSn system as function of changes in volume and electron density.

NFL behaviour.

We summarize the development of magnetism in CeTSn compounds as a function of the two parameters, volume and electron density, in a tentative phase diagram (Fig. 79). Three regions can be distinguished. The paramagnetic range (PM) with enhanced Pauli susceptibility (at best), the strongly disordered magnetic (SDM) region where probably only short range order (spin freezing) is present, and the long range ordered antiferromagnetic (AFM) regime which usually exhibits complex spin arrangements.

CeCuSn

Bulk magnetic data on CeCuSn showed complex and difficult to understand antiferromagnetic ordering below $T_N \approx 8.6\,\mathrm{K}$. A marked dependence on applied fields was observed. In the limit $B \to 0$ the presence of two magnetic phases was deduced. Phase I exists between 8.6 K and 7.4 K, phase II below 7.4 K. Above 8.6 K the material was thought to be paramagnetic. Practically no information is available on the spin structure in the different magnetic phases (i.e. neutron diffraction data have not been reported thus far), but they were all considered to

be antiferromagnetically long-range ordered. The low temperature Sommerfeld constant of CeCuSn is only very slightly enhanced ($\gamma = 32\,\mathrm{mJ}/(\mathrm{mol\,K}^2)$), excluding heavy fermion behaviour, and the relatively large saturation moment of $1.48\,\mu_B$ per formula unit places CeCuSn in the regime of localized $4f$ magnets. Unfortunately, CeCuSn is not a proper endpoint for the series $CeNi_{1-x}Cu_xSn$, since CeNiSn and CeCuSn have quite different crystal structures and their electronic properties cannot simply be compared.

Our μSR studies were carried out on a polycrystalline powder sample used previously in the bulk magnetic study. The results are summarized in the magnetic phase diagram shown in Fig. 80. The presence of two magnetic states is confirmed, but each contains more than one spin system with different types of correlations. The onset of magnetism begins near 11 K. In the temperature range down to 7.5 K a gradual formation of a dynamic (according to LF data) short range correlated (SRC) spin state is seen that coexists with spins keeping their paramagnetic nature. The rate of formation of the SRC state is maximal around 8.5 K, which is probably the reason for the earlier

identification of T_N. At 7.4 K long range ordering of the remaining paramagnetic fraction (having a volume fraction of roughly 20% at all temperatures $T < 7.4\,\mathrm{K}$) takes place. The SRC state is at first unaffected by this ordering process. At lower temperatures it begins to lose its spin dynamics and ends in a spin frozen state around 3.5 K.

Whether the two magnetic surroundings (short and long range ordered) sensed by the muons at $T \ll 7.5\,\mathrm{K}$ reflect a magnetically inhomogeneous material, or whether a homogeneous spin structure with only partially long range ordered spins exists cannot be decided at this stage and calls for magnetic diffraction data. The presence of a SRC spin state explains the strong dependence on applied fields.

CEF induced spin-slip structure in the incommensurate magnetic ordering of CePtSn

While neutron scattering shows incommensurate magnetic Bragg peaks in CePtSn and CePdSn, zero field muon spin relaxation displays well-defined coherent oscillations indicating local commensurate ordering. To reconcile these apparently contradictory results, we had suggested the presence of a spin-slip structure similar to that in holmium metal. Revisiting the neutron scattering data, Kadowaki found some examples of spin-slip structures that are consistent with the neutron results. We have then carried out numerical modelling which shows that, given a simple incommensurate ordering mechanism represented by a spiralling effective field at the cerium sites, the known Ce crystalline electric field (CEF) in CePtSn will generate that kind of spin-slip structure. Further numerical modelling shows that such CEF spin-slip structures generate field distributions at the muon sites with sharp peaks generally consistent with the coherent oscillations observed in our earlier μSR data. CePdSn is likely to behave in a similar manner.

Correlation lengths in inhomogeneously disordered magnets

In several magnetically disordered systems like $CeNi_{1-x}Cu_xSn$, transition metal quasicrystals, or rare earth pyrochlores, static zero-field muon spin relaxation was observed with too shallow a minimum of polarization to be consistent with either a Gaussian or a Lorentzian Kubo-Toyabe function. It had been shown that this anomalous feature can be explained assuming a Gaussian distribution of the width of the Gaussian distribution of the local field used in the Kubo-Toyabe formalism. This new relaxation function was termed 'Gaussian broadened Gaussian' (GBG). Originally, no microscopic physical model for this relaxation function or the underlying distribution of local field was known. The simple notion of an additional random distribution
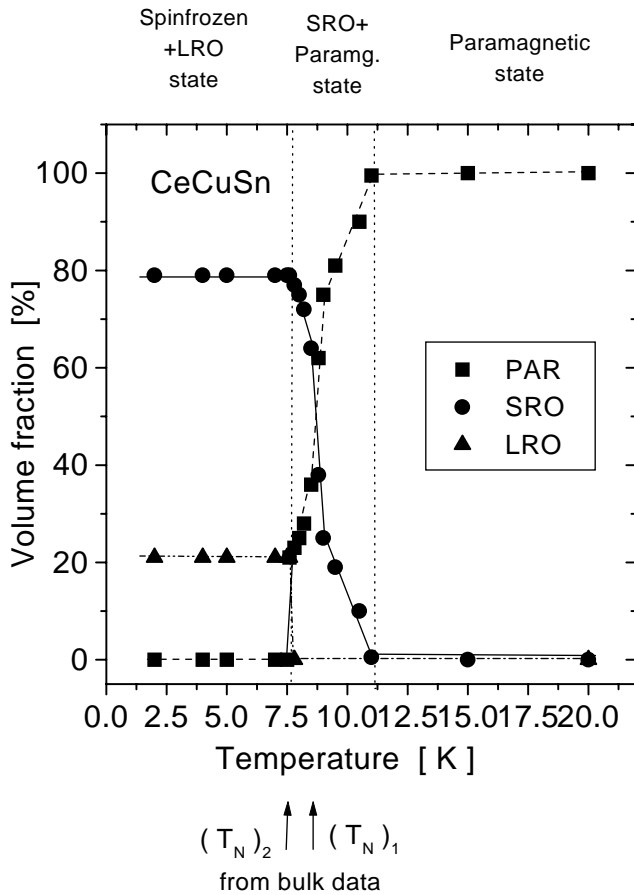

Fig. 80. μSR magnetic phase diagram of CeCuSn. PAR = paramagnetic, SRO = short range ordered, LRO = long range ordered fraction.

of local moment magnitude did not lead to the desired result. Recently, Monte Carlo numerical calculations were able to demonstrate that a model of 'range correlated moment magnitude variation' (RCMMV) will produce the GBG function. In this model the ion moment orientations are completely random with moment magnitude constant within a certain range region, but changing from one region to the next. Hence a shallow static muon spin relaxation function of GBG-type is an indicator for an inhomogeneously disordered magnet. Furthermore, the 'shallowness' of the polarization minimum could be directly related to the correlation length (the typical size) of the regions. The model is quite general, but one obvious application is the inhomogeneous spin disorder in the $CeNi_{1-x}T_xSn$ system, which has been discussed above.

Experiment 804
Muonium in gallium nitride
(R.L. Lichti, Texas Tech)

The group-III nitrides, especially GaN, are important materials for short wavelength opto-electronic applications. Hydrogen impurities play a role in the incorporation of acceptor dopants into the nitrides, and post-growth control of hydrogen is crucial to activating p-type electrical behaviour. This experiment investigates the muonium analogue of isolated hydrogen defect states in GaN in order to gain important knowledge concerning the sites, charge states, stability and diffusive mobility of isolated Mu / H centres. We have previously identified QLCR signals and zero-field relaxation functions characteristic of two inequivalent Ga anti-bonding (AB) sites occupied by Mu^- centres, and have studied the mobility of these states [Lichti *et al.*, Physica **B273-274**, 116 (1999)].

QLCR from Zn-doped GaN

Recently Expt. 804 has investigated partially compensated Zn-doped GaN. This high-resistivity GaN sample was expected to exhibit primarily Mu^+ states rather than the Mu^0 and Mu^- states found in 10^{16} and $10^{18}\,cm^{-3}$ n-type GaN studied previously. Contrary to expectations, the data at room temperature and above proved to be nearly identical in the high-resistivity and standard n-type materials. This result strongly suggests that Mu^- states are primarily formed by capture of electrons from implantation damage. Below 200 K some important differences were observed between the two sample types in the relative signal intensities of observed states.

Figure 81 shows level-crossing data obtained at 30 K and 294 K for GaN:Zn. This sample is over 220 μm thick and has a large cross section, thus essentially all the muons stop in the sample and resonance amplitudes do not require renormalization. The lines at
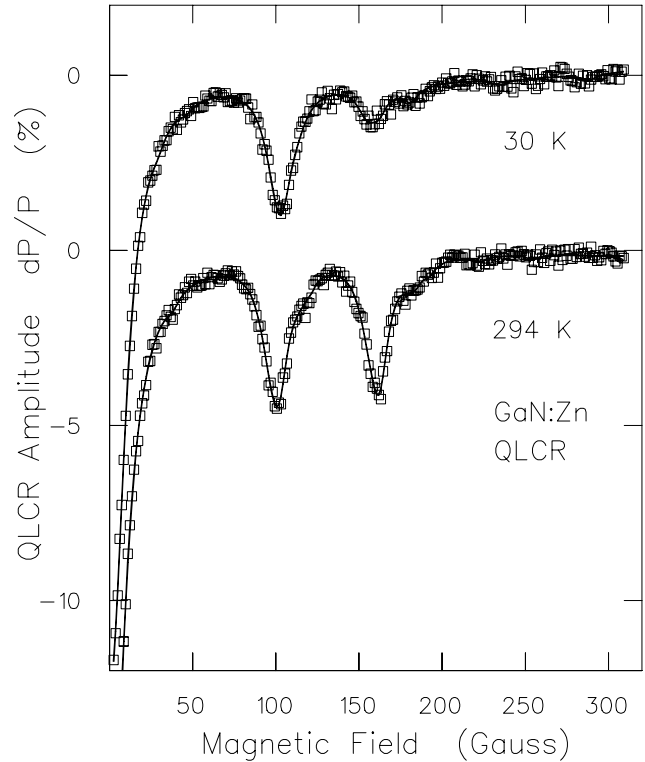

Fig. 81. Level-crossing data from GaN:Zn showing spectra from the three dominant diamagnetic Mu centres observed in both n-type and high resistivity GaN.

zero field fit to nearly the same parameters for the two temperatures, implying that the zero-field relaxation rates will be very similar for the dominant high- and low-temperature states. The room-temperature QLCR spectrum is typical of the Mu^- states previously characterized. The two nearly identical features arise from the two Ga isotopes. The spectrum from the stable site consists of a pair of doublets as expected for AB_{Ga} locations oriented into the wurtzite channel regions at 70° to the c-axis. One doublet of this pair is clearly seen in the 30 K data as the ^{69}Ga related doublet between 120 and 200 G. This signal is present at roughly the same intensity in both displayed spectra. A strong single line per Ga isotope is assigned to a metastable site and implies an nn Ga along the c-axis with the Mu^- located within the cage region of the GaN structure.

The second low-temperature state gives a single strong line near 100 G and lacks the isotopic signature of Ga. This spectrum is assigned to a site near a nitrogen atom and implies a Mu-N "bond" along the c-axis. Such a result is consistent with an AB_N site within the cage, a location which is most likely to be occupied by a Mu^+ centre. There are several additional small amplitude resonances present throughout the investigated temperature range; however, at present no site assignments have been made for any of these much weaker signals.

The 200 K transition

The earlier work on n-type GaN identified a transition near 200 K, observed in both the QLCR and zero-field relaxation data, during which the Mu^- state within the cage region is formed. Much of the recent time was spent investigating this transition region. The nitrogen related QLCR signal intensity decreases while the c-axis Ga related signal grows with increasing temperature over this range. Lorentzian lineshapes were assumed in an effort to obtain more detailed information from the QLCR spectra. Because the ^{71}Ga and N resonances near 100 G strongly overlap, parameters for ^{71}Ga lines were dictated by ratios of Ga isotope properties while those for the ^{69}Ga lines at higher fields and the N resonance were left free in fitting the spectra.

Figure 82 shows the temperature-dependent amplitudes associated with the three identified states based on these fits. The nitrogen related signal associated with Mu^+ centres decreases in two steps. The more rapid decrease starting near 175 K is accompanied by an increase in intensity for both of the Mu^- locations, with the largest fraction staying in the cage region. Additional data are needed to completely map this transition region. However, the present data are sufficient to conclude that the primary initial state associated with these transitions in high-resistivity Zn-doped GaN is Mu^+ at an AB_N site along the wurtzite c-axis, and that the main final states are Mu^- centres which remain trapped within the same cage. Both the N and Ga c-axis oriented cage sites are expected to be metastable locations for their respective Mu charge states. The conclusions from the QLCR data on high resistivity GaN are consistent with a preliminary picture based on zero-field r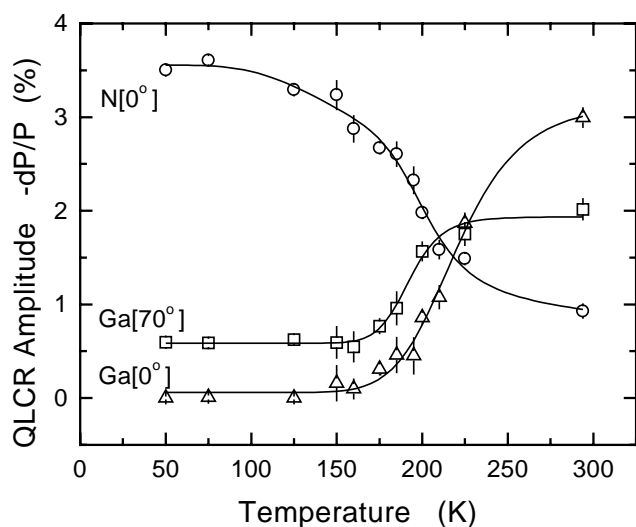elaxation data from Si-doped and unintentionally doped n-type GaN studied previously. A somewhat surprising implication is that the mix of Mu charge states appears to be nearly independent of electron concentration over the range investigated thus far, a much different situation from what is typical of other semiconducting materials.

Experiment 808
Magnets frustrated by competing exchange
(G.M. Kalvius, Tech. Univ. Munich)

Two series of rare earth (RE) intermetallics were investigated to study the effect of competing interactions on the development of long range spin order.

$REFe_6Al_6$

The intermetallics $REFe_6Al_6$ (RE = Tb, Ho, Er) crystallize in the $ThMn_{12}$ structure (space group $I4/mmm$). This lattice contains four different positions denoted as $2a, 8i, 8j,$ and $8f$. Neutron scattering carried out on the same samples used for the μSR study established that the 2a, 8f, 8i sites are fully occupied by RE, Fe, Al ions, respectively, while the 8j site contains Fe and Al ions in random order. Furthermore, all three $REFe_6Al_6$ compounds order ferromagnetically around 340 K, forming ferromagnetic RE and Fe sublattices which are antiferromagnetically coupled. The magnetic Bragg peak intensities, however, show a sluggish increase below T_N, suggesting that the ordering process extends over a wide temperature range (see Fig. 83, upper panel). The likely mechanism preventing normal development of the order parameter is frustration of the spin system by the different intra- and inter-sublattice exchange couplings combined with the local disorder of magnetic ions on the 8j site.

Fig. 82. The temperature dependence of QLCR signal amplitudes from Mu^- channel (Ga[70°]) and cage (Ga[0°]) sites, and Mu^+ cage sites (N[0°]) in Zn-doped GaN.
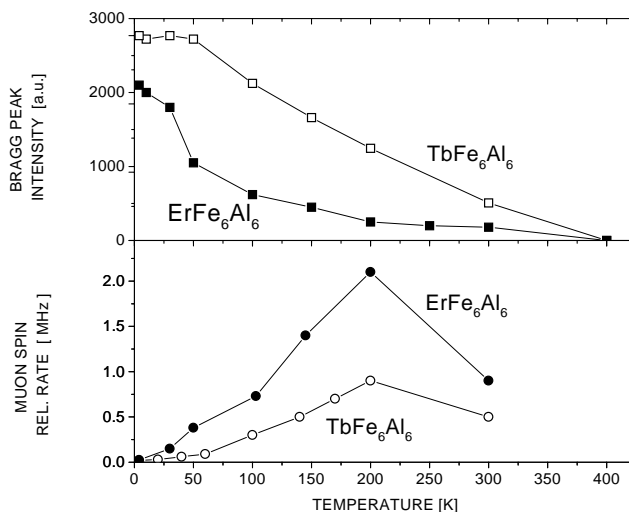

Fig. 83. Temperature dependence of the intensity of the 101/200 Bragg peak (upper panel) and the longitudinal (dynamic) muon spin relaxation rate (lower panel) for $ErFe_6Al_6$ and $TbFe_6Al_6$. All lines are guides to the eye.

Our μSR data show at all temperatures below T_N the spectral response typical for magnetically-ordered powder samples:

$$\mathcal{A}(t) = (2A_0/3)\exp(-\Lambda_t t)\cos(\nu_\mu t) + (A_0/3)\exp(-\lambda_l t).$$

Spin-glass behaviour is not observed, but it is found that $\Lambda_t \ll \nu_\mu$, which indicates substantial disorder in the spin lattice. The longitudinal rate λ_l, sensing spin dynamics alone, reveals that quasi-static LRO is attained only below ~ 50 K, that is far below T_N. The lower panel of Fig. 83 depicts the situation. We conclude that this persistent spin-dynamical behaviour causes the sluggish approach to saturation of Bragg peak intensity. Further, a peak in longitudinal relaxation rate around 200 K is apparent. This probably reflects a delayed ordering of the Fe ions on the disordered 8j site. It could also be caused by the onset of muon dynamics, but data on other compounds having the same lattice structure show that the muon is static at least up to room temperature.

In summary, the main effect of frustration in the RE and Fe magnetic sublattices is the persistence of spin dynamics deep into the LRO state which is characterized by substantial local spin disorder. Nonetheless, the frustration is not strong enough to prevent long-range order altogether.

RETC$_2$

The rare earth-transition metal (T) dicarbides have the crystallographic space group $Amm2$. They order ferromagnetically for T = Co and antiferromagnetically (with a rotation of the easy axis by 90°) for T = Ni. One can prepare mixed systems of the type TbCo$_x$Ni$_{1-x}$C$_2$. In these materials the ferromagnetic exchange competes with the antiferromagnetic exchange together with the different CEF couplings for the two orientations of the easy axis. This situation leads to three magnetic states: ferromagnetism, amplitude modulated magnetism, and normal collinear antiferromagnetism. The modulated state always forms the magnetic ground state. The present μSR results indicate strong local spin disorder and persistent spin dynamics in the different LRO magnetic states for three compounds studied ($x = 0.3, 0.5, 0.7$). Details depend on the value of x as demonstrated by Fig. 84. The Ni-rich material (small x) shows more pronounced spin dynamics, the Co-rich material (large x) enhanced spin disorder. Neutron diffraction data indicate a small effective moment in the AFM state. This is considered a consequence of the persistent (longitudinal) spin fluctuations. Again the effect of frustration is visible in the local magnetic parameters sensed by μSR, but long-
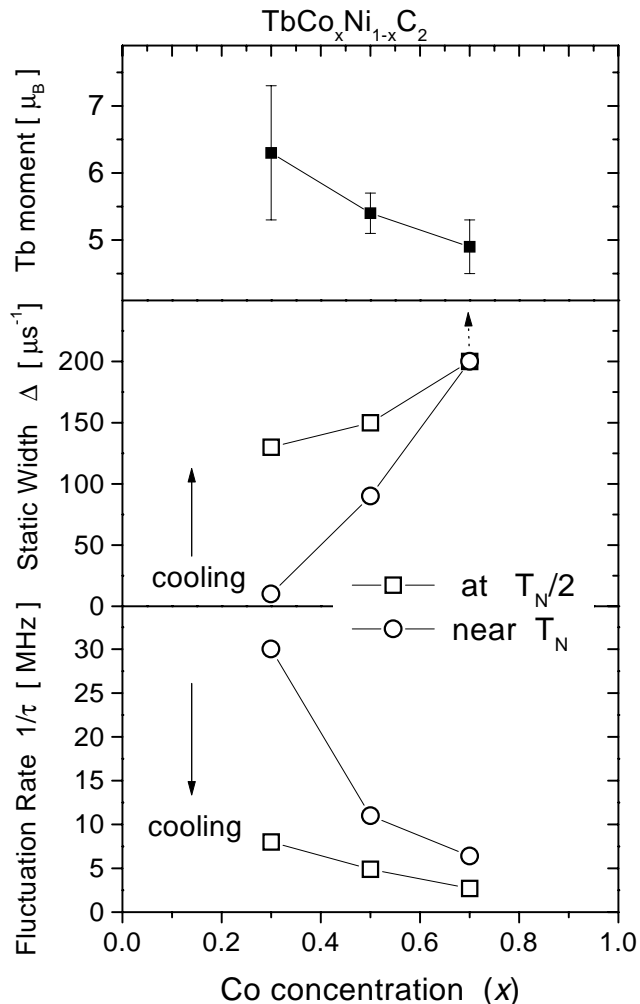

Fig. 84. Comparison of different ZF-μSR parameters for the modulated spin states in TbCo$_x$Ni$_{1-x}$C$_2$ near and well below the ordering temperature T_N as a function of x together with the magnitude of the ordered moment obtained from neutron scattering. All lines are guides to the eye.

range magnetic order cannot be suppressed. Furthermore, we found no indication for a spin-glass-like magnetic precursor state above T_N or T_C.

Experiment 834
μSR study of transverse spin freezing in bond-frustrated magnets
(D.H. Ryan, McGill)

The random addition of antiferromagnetic (AF) exchange interactions to an otherwise ferromagnetic (FM) system leads to a loss of FM order through exchange frustration. In extreme cases, a spin glass (SG) is formed with random isotropic spin freezing and neither net magnetization nor long range order. At lower levels of frustration the system exhibits characteristics of both extremes as long-ranged FM order co-exists with SG order in the plane perpendicular to the FM order. On warming such a system from $T = 0$ K, the

SG order first melts at T_{xy} followed by the loss of FM order at T_c. This picture has emerged from mean field calculations, numerical simulations and experimental measurements.

The aim of the current series of experiments is to investigate the magnetic behaviour in the region of T_{xy} in some partially frustrated alloys. Specifically, numerical simulations predict that although the freezing of transverse spin components does not represent a phase transition, it should be accompanied by significant, but non-critical, magnetic fluctuations. A direct search for such fluctuations in χ_{ac} is complicated by the dominant response of the FM order; however, the two contributions are easily distinguished using muons. μSR provides an additional advantage in that it can be performed without applying an external magnetic field that might be expected to perturb the magnetic behaviour.

The system chosen for the first run in December, 1998 was a $-Fe_xZr_{100-x}$. The magnetic behaviour in this binary alloy can be tuned from FM to close to the FM–SG crossover boundary at a critical composition of $x_c \sim 93$ at.% simply by varying the iron content.

The dynamic relaxation rates shown for each alloy in Fig. 85 clearly illustrate the evolution from ferromagnet at $x = 89$ to spin glass at $x = 93$. T_c is marked by a clear cusp in $\lambda(T)$ that moves down in temperature as the frustration level increases. At the same time, a broad feature develops at a much lower temperature for $x \geq 90$. This peak both grows in amplitude and moves to higher temperatures with increasing x and hence frustration. Finally the two features merge at $x = 93$ as the system becomes a spin glass. These results are in perfect accord with both qualitative descriptions of transverse spin freezing and numerical simulations which predicted a broad, non-critical, fluctuation peak at T_{xy} as the transverse spin components order. A second clear prediction of transverse spin freezing models is an increase in the net ordered moment below T_{xy} as the transverse components add to the ferromagnetic order established at T_c. This effect was clearly visible in the temperature dependence of the static signal.

The results of our analysis of $\lambda(T)$ and $\Delta(T)$ are summarized as a phase diagram (Fig. 86). The agreement between the static and dynamic μSR signatures and also χ_{ac} data confirms that we are indeed detecting the onset of order at T_c. Furthermore, $\lambda(T)$ and $\Delta(T)$ also yield the same value for T_{xy} in each case (the average deviation is less than 5 K), clearly demonstrating that the lower fluctuation peak is also associated with changes in the static order, as predicted by numerical simulations. In all cases, however, T_{xy} is more easily identified from the peak in λ than from the break in
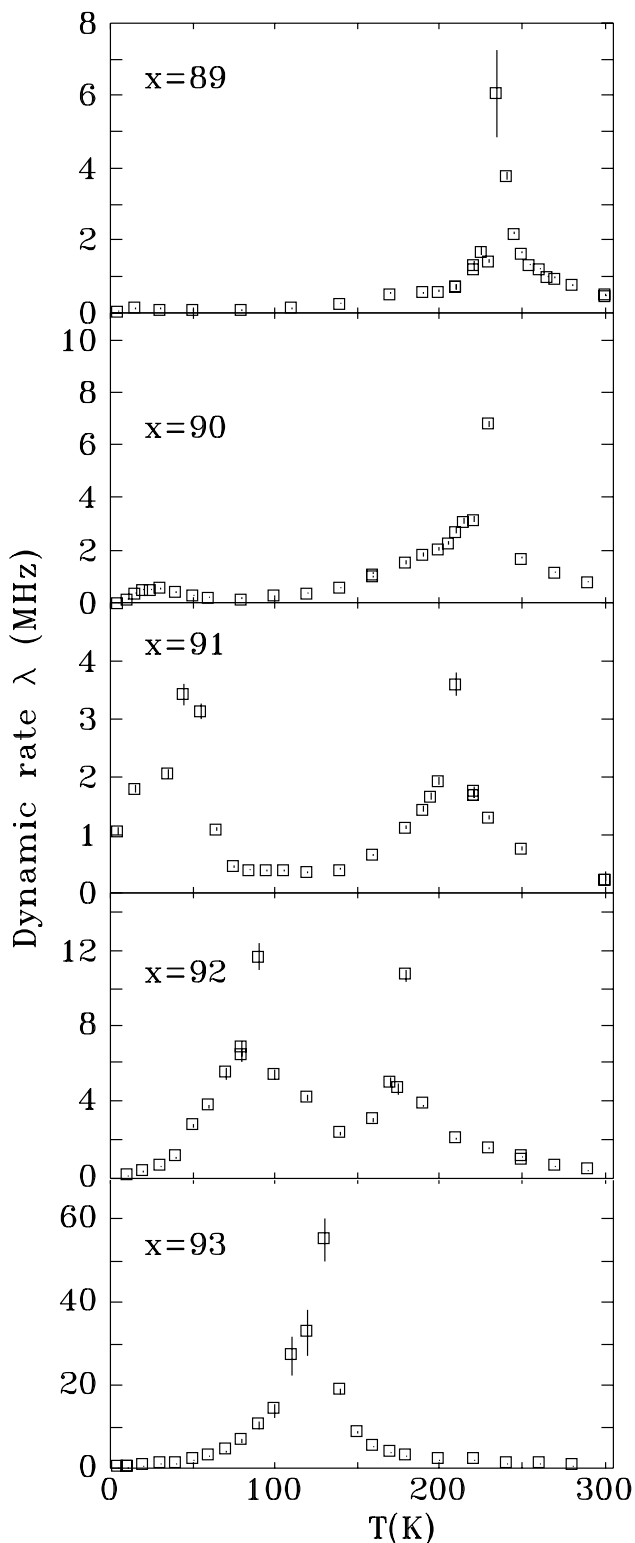

Fig. 85. Temperature dependence of the dynamic relaxation rate (λ) showing the high temperature cusp (T_c) merging with the lower temperature feature (T_{xy}) with increasing frustration.
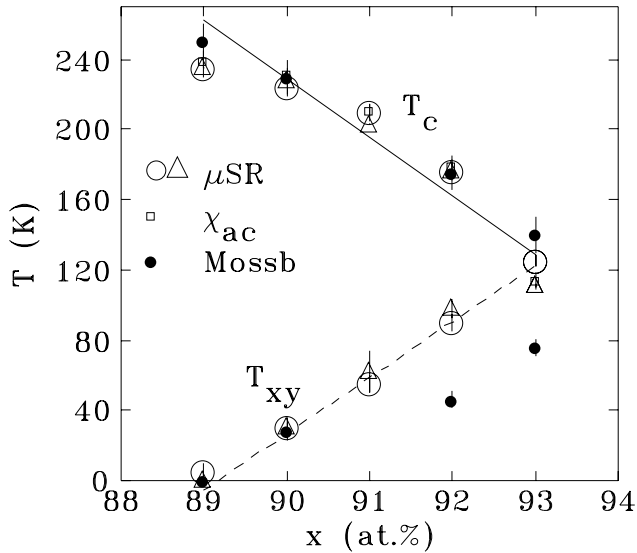
Fig. 86. Magnetic phase diagram for a $-Fe_xZr_{100-x}$ showing T_c and T_{xy} deduced from μSR data. Open circles mark values derived from the peak in λ, while the open triangles reflect values derived from fitting $\Delta(T)$. T_cs derived from χ_{ac} measurements on the same samples are also shown as small open squares. Values obtained on an independently prepared series of alloys and measured using applied-field Mössbauer spectroscopy are shown for comparison as solid symbols.

$\Delta(T)$, underlining the benefits of using μSR to study transverse spin freezing. One unexpected result was the discrepancy between the Mössbauer and μSR values for T_{xy} as x increased to 93. The Mössbauer results are systematically lower and we believe that this is related to applied fields used in the Mössbauer work.

Present status of Expt. 834

In December, 1999, we carried out some preliminary measurements on a $-Fe_{90-x}Ru_xZr_{10}$, a related system that should provide better access to the FM–SG crossover region. Instrumental problems with the data acquisition system have delayed analysis of these data. We have been allocated another 2 week run for this summer. This run will be used to examine the FM–SG crossover region in more detail in a $-Fe_xZr_{100-x}$, and also to measure the field dependence of T_{xy} which is both predicted by mean field models, and also inferred from a comparison of the μSR and Mössbauer values for T_{xy} shown in Fig. 86.

Experiment 844
Quantum impurities in one dimensional spin 1/2 chains
(J. Chakhalian, R. Kiefl, UBC/TRIUMF)

The goal of Expt. 844 is to test recent predictions on the effect of quantum impurities in quasi one dimensional spin 1/2 antiferromagnets $KCuF_3$ and CPC ($CuCl_2N\cdot(C_5D_5)$). Unlike integer spin 1-D chains

where low energy excitations exhibit a well-known Haldane gap, the half-spin chains have a gapless excitation spectrum. Unusual quantum phenomena are predicted when a non-magnetic impurity perturbs the spin 1/2 chain as a result of the gapless bulk excitations in a spin 1/2 case. The effect is somewhat analogous to the well-known Kondo effect when a magnetic impurity interacts with conduction electrons in a metal which is understood in terms of Fermi liquid theory [Henson, *The Kondo Problem to Heavy Fermions* (Cambridge Univ. Press, 1993)].

Recent advances in conformal field theory have led to new interesting predictions on the local susceptibility in the vicinity of a single quantum impurity in quasi-1D S=1/2 antiferromagnetic chains [Eggert and Affleck, Phys. Rev. **B46**, 10866 (1992); Eggert, UBC Ph.D. thesis, unpublished; Affleck and Ludwig, Nucl. Phys. **360**, 641 (1991); Ludwig and Affleck, Phys. Rev. Lett. **67**, 3160 (1991); Affleck and Ludwig, Phys. Rev. **B48**, 7297 (1993)]. It was found that the effects of a non-magnetic impurity can propagate deep into the chain a distance which is essentially determined by the strength of coupling between neighbouring ions. Remarkably the effects are different if the perturbing species is symmetrically placed between two magnetic ions or symmetric about the site of an ion.

The positive muon provides an ideal realization of an isolated impurity in the chain since there is only one muon in the target at a time. Furthermore the local spin susceptibility can be probed easily using the technique of muon spin rotation. The main perturbation in this system arises from the muon charge. The effect of the perturbed links is reflected in the muon paramagnetic frequency shift or Knight shift thus providing an excellent test for the theory. Figure 87 shows preliminary results of our μSR Knight shift measurements performed on the powder sample of CPC at the field of 4 kG.

As we expected, the muon charge significantly disturbs the coupling between ions. The measured muon Knight shift is substantially different from the unperturbed CPC chain susceptibility. To explain the observed paramagnetic shift we performed fast Fourier transformation (FFT) of our timing spectra. The resulting Fourier spectra revealed a significant difference in muon behaviour in low and high temperature regions. At temperatures above 20 K we observed a single frequency line which indicates that muons are immobile on the μSR timescale and experience the same hyperfine field (see Fig. 88). At low temperatures (below 20 K), the single frequency line becomes noticeably broad and eventually splits into 3 lines as the temperatures drops below 7.5 K (see Fig. 89). The frequency splitting indicates there is more than one magnetically
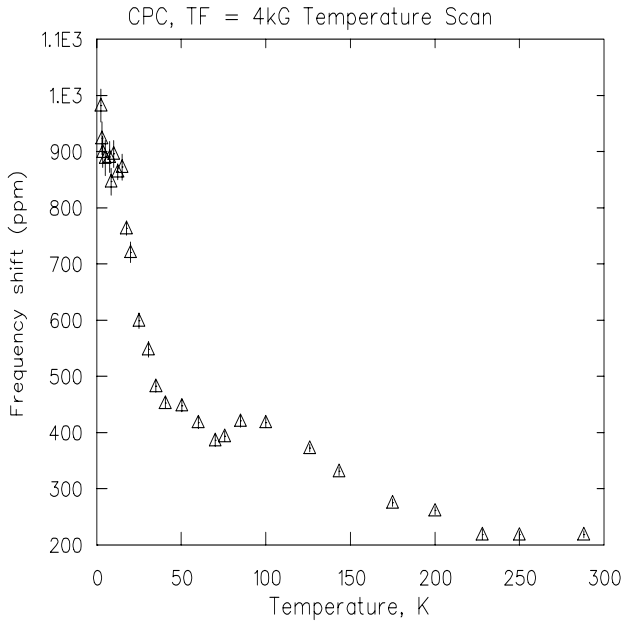
Fig. 87. CPC temperature dependent Knight shift measured in a magnetic field of 4 kG.

inequivalent site. Note the small peak in the Knight shift data around 100 K which may be an indication of the site change above 100 K (see Fig. 87).

We also performed LF measurements on the CPC sample in a magnetic field of 500 G. Figure 90 shows the results of our preliminary analysis. As was the case with the Knight shift, the longitudinal relaxation rate $1/T_1$ also exhibits very unusual behaviour largely attributed to a broken or perturbed spin chain [Brunel *et al.*, e-print cond-mat/9902028]. One of the most
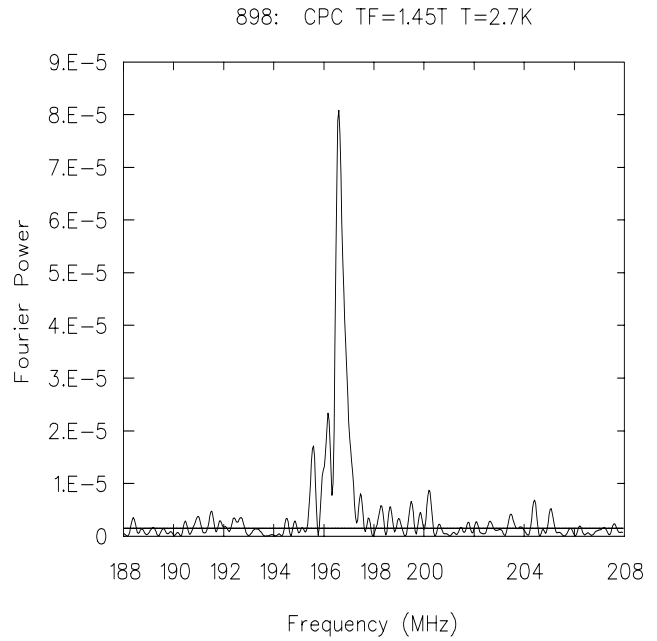

Fig. 89. As the temperature decreases the single line splits into 3 distinct frequencies, possibly indicating that muons sample different sites.

interesting theoretical predictions is on the $1/T_1$ rate at the edge of the broken chain. Unlike a bulk case of an unbroken chain where $1/T_1 \sim \log^{1/2} T$, a comformal theory predicts a very different $1/T_1$ temperature dependence $1/T_1 \sim T \log^2 T$ for the broken 1-D spin 1/2 chain.
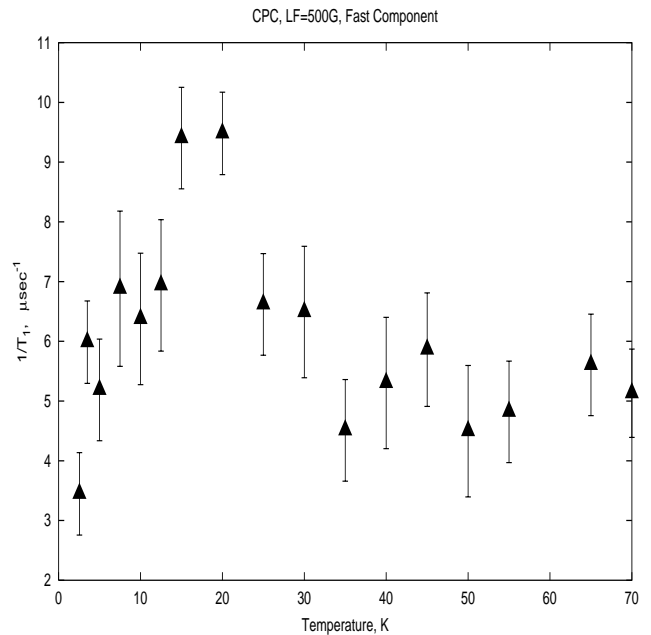

Fig. 88. Single frequency line observed at high temperatures indicates that muons are essentially immobile.

Fig. 90. $1/T_1$ relaxation rate measured in LF of 500 G on CPC sample.

Experiment 846
Complex order parameter symmetry in YBa$_2$Cu$_3$O$_{7-\delta}$ at low T and high magnetic field
(J.H. Brewer, TRIUMF/UBC; J.E. Sonier, LANL)

In 1999 we performed a transverse field μSR study of the vortex state in YBa$_2$Cu$_3$O$_{7-\delta}$ single crystals using the Belle spectrometer on the M15 beam line. The aim was to investigate the nature of the pairing symmetry in high-T_c cuprate superconductors at high magnetic fields, where other experiments have reported anomalous behaviour. In particular, scanning tunneling spectroscopy (STS) measurements in YBa$_2$Cu$_3$O$_{7-\delta}$ [Maggio-Aprile *et al.*, Phys. Rev. Lett. **75**, 2754 (1995)] and thermal conductivity measurements in Bi$_2$Sr$_2$CaCu$_2$O$_8$ [Krishana *et al.*, Science **277**, 83 (1997); Aubin *et al.*, Science **280**, 9a (1998)] and underdoped YBa$_2$Cu$_3$O$_{6.63}$ [Ong *et al.*, cond-mat/9904160] showed features at high magnetic field that are seemingly inconsistent with the established $d_{x^2-y^2}$-wave pairing symmetry in these compounds. A field-induced transition from a $d_{x^2-y^2}$-wave state to a fully gapped state, such as $d_{x^2-y^2} + id_{xy}$ or $d_{x^2-y^2} + is$, had been offered as a possible explanation for these results [Laughlin, Phys. Rev. Lett. **80**, 5188 (1998); Franz and Tešanović, Phys. Rev. Lett. **80**, 4763 (1998)]. However, our measurements of the magnetic penetration depth $\lambda_{ab}(T,H)$ in YBa$_2$Cu$_3$O$_{6.95}$ show that this region of the vortex phase is consistent with a pure $d_{x^2-y^2}$-wave order parameter in which previously unobserved nonlinear and nonlocal effects produce the observed variation with field and temperature.

Figure 91 shows the temperature dependence of λ_{ab}^{-2} (which is proportional to the density of superconducting carriers) at $H = 0.5$, 4 and 6 T in detwinned single crystals of YBa$_2$Cu$_3$O$_{6.95}$. The solid curve, which agrees very well with the $H = 0.5$ T data at low
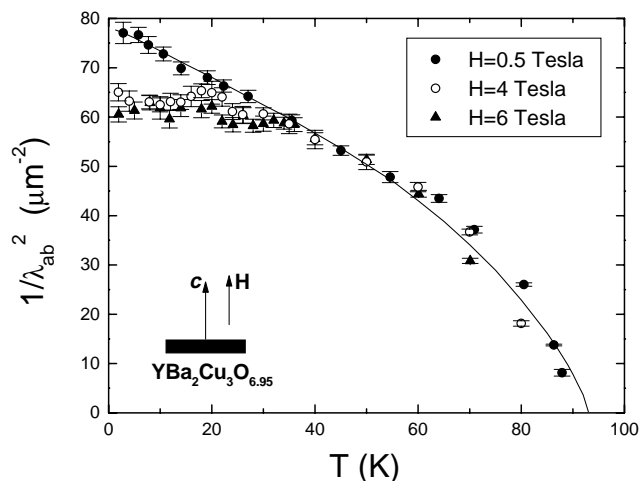

Fig. 91. Temperature dependence of λ_{ab}^{-2} at $H = 0.5$ T, 4 T and 6 T. The solid curve represents the zero-field microwave measurements of $\Delta\lambda_{ab}(T)$.
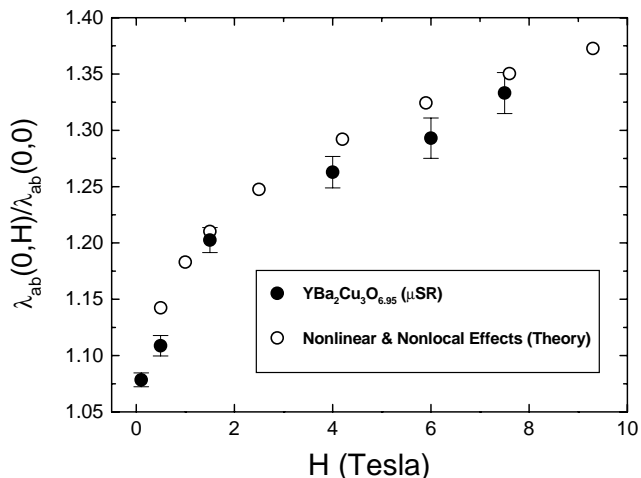

Fig. 92. Magnetic field dependence of λ_{ab} extrapolated to $T = 0$ K (solid circles) compared to that predicted for non-local and nonlinear effects in the vortex state of a pure $d_{x^2-y^2}$-wave superconductor (open circles) [Amin, Affleck and Franz, Phys. Rev. **B58**, 5848 (1998)].

T, represents microwave measurements of $\Delta\lambda_{ab}(T)$ at zero DC field [Hardy *et al.*, Phys. Rev. Lett. **70**, 3999 (1993)] converted to λ_{ab}^{-2} using the μSR value of λ_{ab} at $T = 1.35$ K. The linear T-dependence of λ_{ab}^{-2} at low temperature and $H = 0.5$ T is characteristic of a superconducting order parameter which has $d_{x^2-y^2}$-wave symmetry (rather than s-wave symmetry as in conventional superconductors). At $H = 4$ and 6 T, the linear T-dependence at low temperatures vanishes and the magnitude of λ_{ab}^{-2} is substantially reduced.

The magnetic field dependence of λ_{ab} extrapolated to $T = 0$ K agrees extremely well with the theoretical prediction for the *nonlocal* and *nonlinear* supercurrent response of a pure $d_{x^2-y^2}$-wave superconductor in the vortex state (see Fig. 92). Our measurements are the first clear observation of nonlocal and nonlinear effects in the vortex state of a high-T_c superconductor. Furthermore, our findings provide strong evidence that the symmetry of the superconducting order parameter at high field is unaltered from the well-established $d_{x^2-y^2}$-wave symmetry at low and zero field.

Experiment 846 was a new proposal in December 1998, which together with Expt. 847 and Expt. 848 replaced Expt. 691. We plan to continue the investigation of the pairing symmetry in YBa$_2$Cu$_3$O$_{7-\delta}$ by exploring other regions of the H-T phase diagram for this material.

Experiment 848
μ^+SR studies in YBa$_2$Cu$_3$O$_{7-x}$
(R.I. Miller, R.F. Kiefl, TRIUMF/UBC)

Experiment 848 was established in 1999 to continue the investigation of the YBCO family of Type II, high temperature superconductors. Our goal was to inves-

tigate the underdoped YBCO compound and measure the vortex lattice in this material.

YBCO$_{6.5}$ – penetration depth measurements

Preliminary analysis of μ^+SR data taken in the vortex state of YBCO$_{6.5}$ shows low temperature behaviour of the penetration depth to be unconventional. Figure 93 shows the temperature dependence of the penetration depth. The penetration depth is extracted from fits to the μ^+SR polarization function, based on a theoretical model of the field distribution in the vortex lattice.

Figure 94 shows the variation in the absolute value of the penetration depth as a function of oxygen concentration, for similar applied fields (H = 5 kG) and temperature ranges. In all 3 samples the penetration depth exhibits temperature dependence far below T_c.

Finally, Figs. 95 through 97 show the Fourier transform of the polarization signal in YBCO$_{6.95}$, YBCO$_{6.6}$ and YBCO$_{6.5}$ at T = 2.5 K and H = 5 kG. Clearly the superfluid density decreases dramatically from an oxygen doping of 6.95 to 6.5.

754: Big YBCO6.95 Xtal, TF=0.5T, T=2.7K [1,2,3,4]
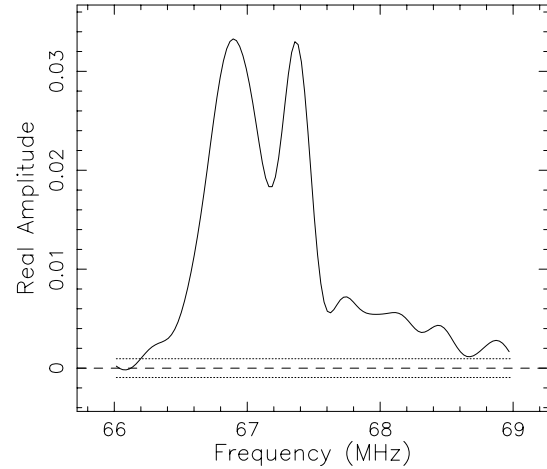
Fig. 95. FFT of the muon polarization signal in YBCO$_{6.95}$ in an applied field of H = 5 kG and T = 2.5 K.

6217: Dtw YBCO66 TF=5kG T=2.4K [1,2,3,4] RRF

Fig. 96. FFT of the muon polarization signal in YBCO$_{6.60}$ in an applied field of H = 5 kG and T = 2.5 K.

724: YBCO6.5 ortho2 TF=4.8kG T=2.9K [1,2,3,4] R
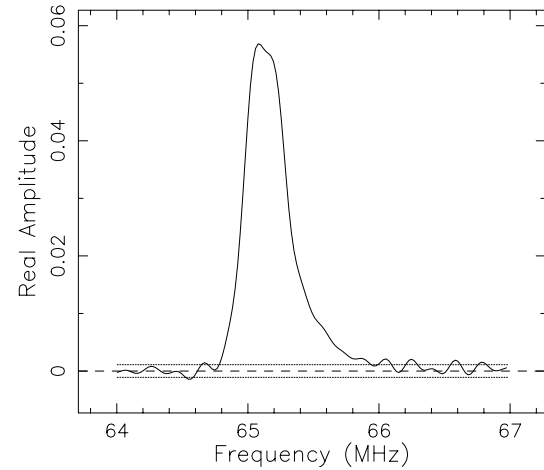
Fig. 97. FFT of the muon polarization signal in YBCO$_{6.50}$ in an applied field of H = 5 kG and T = 2.5 K.
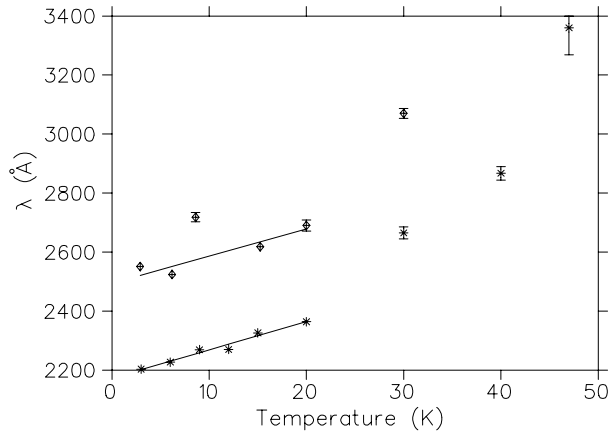

Fig. 93. Temperature dependence of the penetration depth in YBCO$_{6.5}$ in an applied field of H = 2 kG (lower points) and H = 5 kG (higher points).
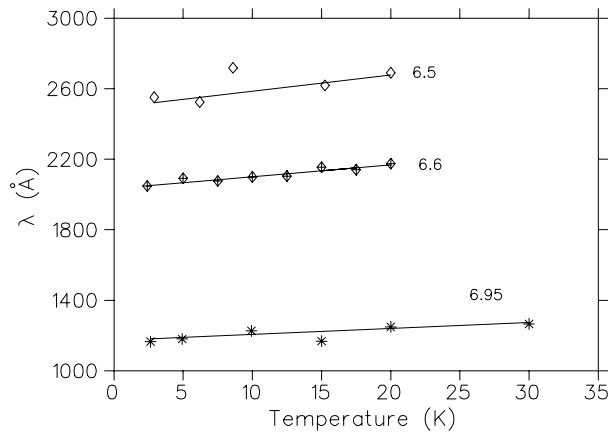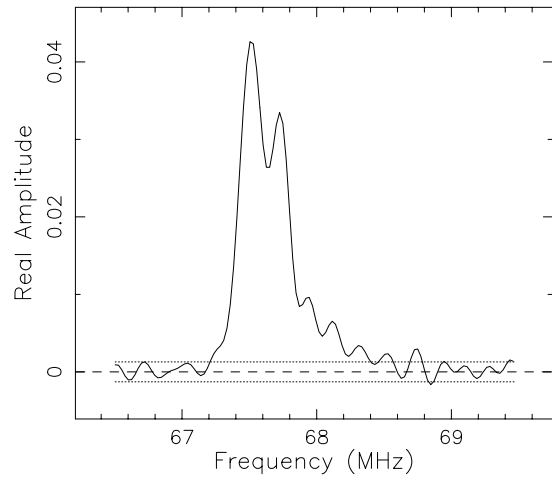

Fig. 94. Temperature dependence of the penetration depth in YBCO for varying oxygen concentrations in applied field of H = 5 kG.

81

YBCO$_{6.5}$ – antiferromagnetic cores?

In Zhang's SO5 theory, unifying antiferromagnetism and superconductivity in the underdoped high temperature superconductors, a suggestion is made that the vortex cores may exhibit antiferromagnetism in a high applied magnetic field. We have attempted to phenomenologically model the effect of such antiferromagnets by assuming that implanted muons see enhanced or reduced local fields due to the moments. Very preliminary analysis suggests that μ^+SR polarization signals may provide some evidence for such moments.

Conclusion

Further studies of the penetration depth in YBCO$_{6.5}$ will be undertaken in the spring of 2000. We intend to determine the low field, low temperature value of the penetration depth in both YBCO$_{6.5}$ and YBCO$_{6.95}$.

Furthermore, we will repeat experiments on YBCO$_{6.5}$ at higher fields in the Belle spectrometer to further test Zhang's SO5 theory.

Experiment 851
μSR in ruthenate and cuprate superconductors
(C.E. Stronach, Virginia State)

We report on a muon spin rotation/relaxation (μSR) study of the superconducting perovskite compound Sr$_2$YRu$_{1-u}$Cu$_u$O$_6$ ($u = 0.05$, 0.10, 0.15) with so little Cu that CuO$_2$ planes do not form. The experiments were performed on the TRIUMF M20 beam line with the LAMPF apparatus in April.

In the high-T_c oxides, the implanted μ^+ particles tend to be trapped near the oxygens. In Sr$_2$YRuO$_6$ there exist three inequivalent oxygen sites: two in the YRuO$_4$ layer [O(1,2) – the O(1) and O(2) sites are only slightly different], and one in the SrO layer [O(3)]. From this we predict the existence of two distinct muon sites, and expect to observe a two-component μSR signal. Polycrystalline Sr$_2$YRu$_{1-u}$Cu$_u$O$_6$ samples were prepared by the standard solid-state reaction, and structural characterization by X-ray diffraction and neutron scattering confirmed stoichiometry and phase homogeneity. Impurity phase was less than 1%. Standard TD μSR was employed, with a veto system that virtually eliminated background signals.

Below 30 K both the ZF and TF spectra indicate two components, reflecting the expected two distinct muon sites. In ZF, the YRuO$_4$ layer sites exhibit fast relaxation and a local magnetic field of about 3 kG. On the other hand, the SrO sites show neither significant relaxation nor a locally-ordered field. The very fast relaxation of the μ^+ at the YRuO$_4$ sites reflects a strong disordering of the Ru moments. When combined with neutron scattering data, a picture emerges of in-plane freezing of Ru spins with the average polarization reversing direction from one YRuO$_4$ layer to the next, thereby presenting a zero field at the μ^+ site in the SrO layer. Upon application of a 500 G TF, the YRuO$_4$ μ^+ sites display rapid muon spin depolarization and a large local magnetic field, while the SrO μ^+ site clearly exhibits a tenfold rise in the relaxation rate λ as the temperature decreases from 30 to 2 K, along with a concomitant diamagnetic shift – consistent with superconductivity. Interestingly, when the magnetic field is removed in a field-cooled sample, we see little evidence of trapped flux, indicating very weak flux pinning. This may be a consequence of near-zero vortex coupling between superconducting layers (isolated sheets of "pancake" vortices), which is consistent with the superconducting hole condensate residing in the SrO layers.

The charge-reservoir oxygen (CRO) model assigns the hole condensate to the reservoir layers (SrO layers in these materials). Its pairing is conventional BCS-like, but allows for electronic as well as photonic pairing, and puts the holes in the SrO layers. Significant predictions of the model include: (i) Ba$_2$GdRu$_{1-u}$CuO$_6$ should not superconduct, (ii) the undercharged oxygen ions that carry the primary supercurrent are in the SrO layers, where there is no large average magnetic field, (iii) the μ^+SR signal amplitude from the SrO layers will be weaker than that from the YRuO$_4$ layers because the holes (repulsive to μ^+) reside primarily in the SrO layers where the oxygen ions are not fully charged to O^{-2}, and (iv) the superconducting carriers are holes so the Hall coefficient should be positive. The present results support this model.

It may not be a coincidence that the in-plane static magnetic ordering of the Ru moments and the fully developed superconductivity in the SrO layers both occur at about 30 K. We further posit that the intrinsic T_c (i.e., in the absence of fluctuating magnetic moments) of the superconducting condensate may be higher, but the rapid fluctuations of the Ru magnetic moments above T_N may suppress the superconducting state. When the temperature is decreased below T_N, the fluctuations cease and the in-plane magnetic ordering (with average polarization reversing direction from one YRuO$_4$ layer to the next) is established. This unique magnetic state (which provides a zero net magnetic field in the SrO layers) may no longer inhibit hole pairing, but does result in the fully developed superconductivity in the SrO layers. Our results are consistent with a ferromagnetic YRu$_{1-u}$CuO$_4$ layer in which the magnetization lies in the a-b plane and reverses direction from magnetic layer to magnetic layer, producing a net antiferromagnetic ordering. While these results are completely consistent with the predictions

of the charge-reservoir oxygen model, we cannot absolutely rule out the possibility of exotic superconductivity with higher-order pairing in the $YRuO_4$ layers.

A paper on this work has already been published in the International Journal of Modern Physics [**B13**, 3670 (1999)]. A shortened manuscript describing this work has also been accepted for publication in the Proceedings of the Eighth International Conference on Muon Spin Rotation, Relaxation and Resonance [Physica B (1999)].